

# A Spectroscopic and Electrochemical Study of Chlorotitanates in Molten Salt Media

by

Luis A. Ortiz

S.B. Materials Science and Engineering  
Massachusetts Institute of Technology, 1996

Submitted to the Department of Materials Science and Engineering  
in partial fulfillment of the requirements  
for the degree of

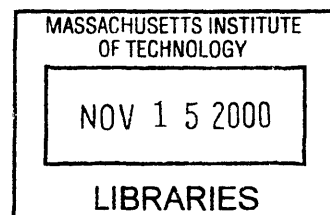
DOCTOR OF SCIENCE IN MATERIALS ENGINEERING

at the

Massachusetts Institute of Technology

June 2000

© 2000 Massachusetts Institute of Technology  
All rights reserved



SIGNATURE OF AUTHOR: \_\_\_\_\_

Department of Materials Science and Engineering  
April 28, 2000

CERTIFIED BY: \_\_\_\_\_

Donald R. Sadoway  
John F. Elliott Professor of Materials Chemistry  
Thesis Supervisor

ACCEPTED BY: \_\_\_\_\_

Carl V. Thompson  
Stavros Salapatas Professor of Materials Science & Engineering  
Chair, Departmental Committee on Graduate Students



# A Spectroscopic and Electrochemical Study of Chlorotitanates in Molten Salt Media

by

**LUIS A. ORTIZ**

Submitted to the Department of Materials Science and Engineering  
on April 28, 2000 in Partial Fulfillment of the  
Requirements for the degree of Doctor of Science in  
Materials Engineering

## *ABSTRACT*

Ultra-high purity titanium is used as a barrier metal in integrated circuitry. Metallothermic reduction does not produce titanium sufficiently pure for micro-electronics applications so electrorefining of the metal in a molten chloride bath at temperatures above 700°C is necessary.

The present study focused on the electrorefining of titanium in a bath consisting of the CsCl-NaCl-KCl eutectic as the solvent. Interfacial phenomena (multiple reaction steps and the kinetics associated with each) related to the faradaic process were investigated with electroanalytical techniques. The bulk chemistry of the electrolyte (the structure of the chlorotitanate complexes) that describes the nature of the species present during the electrorefining process was investigated using spectroscopic techniques. Recommendations were made concerning the potential for the various technologies to be used for on-line control to improve operating practices.

Electrode kinetics were studied by ac voltammetry. Phase angle information was used to determine the value of the standard rate constant ( $k^0$ ) and the transfer coefficient ( $\alpha$ ) for the reduction couples  $\text{Ti}^{3+}/\text{Ti}^{2+}$  and  $\text{Ti}^{2+}/\text{Ti}^0$  at a glassy carbon electrode. The reduction from  $\text{Ti}^{2+}$  to metal has been identified as the slow step in the electrorefining process. The utility of electrochemical sensing to observe concentration changes has been judged poor. Industrial use of reference electrodes is recommended for controlling the overpotential in the electrorefining process and to improve efficiency.

Absorption spectroscopy has established that a temperature sensitive equilibrium between  $\text{TiCl}_6^{3-}$  and  $\text{TiCl}_4^-$  exists in the CsCl-NaCl-KCl eutectic. Fiber optic absorption spectroscopy was shown to be capable of detecting additions of  $\text{Ti}^{2+}$  to melts containing  $\text{Ti}^{3+}$ , as well as sensing  $\text{Ti}^{3+}$  concentration fluctuations at a level of  $\pm 5\text{mM}$ . Raman spectroscopy was found to be ill suited for investigating complexation in this system due to the deeply colored nature of the melts.

Thesis Supervisor: Donald R. Sadoway

Title: John F. Elliott Professor of Materials Chemistry

# Table of Contents

<b>TABLE OF FIGURES.....</b>	<b>6</b>
<b>ACKNOWLEDGEMENTS .....</b>	<b>8</b>
<b>1.0 INTRODUCTION.....</b>	<b>10</b>
1.1 Background.....	10
Titanium metallurgy.....	10
Commercial significance of high purity titanium .....	11
From commercially pure to ultra-high purity.....	13
ALTA flow process.....	14
Existing methods for tracking process chemistry .....	15
1.2 Scope of the present study .....	17
1.3 Organization .....	18
<b>2.0 ELECTROANALYTICAL CHEMISTRY .....</b>	<b>19</b>
2.1 Summary.....	19
2.2 Background.....	19
2.3 Earlier Work .....	25
Electrochemistry.....	25
Physical Chemistry.....	26
Sweep potential experiments with questionable electrodes .....	27
Titanium reduction pathways in different electrolytes.....	27
Recent electroanalytical studies of Ti <sup>3+</sup> including AC methods .....	28
2.4 Experimental/Apparatus/Techniques.....	31
2.5 Results .....	37
2.6 Discussion.....	42
2.7 Summary of Scientific Findings.....	51
<b>3.0 SPECTROSCOPY .....</b>	<b>52</b>
3.1 Summary.....	52
3.2 Background.....	52
3.3 Earlier Work .....	54
Raman investigations of titanium ions in low temperature melts and solid state .....	54
UV/Visible/IR studies of titanium complexation.....	56
Fiber optic investigation of the Raman response in high temperature corrosive melts .....	58
3.4 Experimental/Apparatus/Techniques.....	60
3.5 Results .....	63
Raman Spectroscopy.....	63
Absorption Spectroscopy .....	66
3.6 Discussion.....	71
3.7 Summary of Scientific Findings.....	77

<b>4.0 SENSOR RECOMMENDATIONS.....</b>	<b>78</b>
4.1 Possible Technologies .....	78
Electrochemical.....	78
Raman spectroscopy.....	79
Absorption spectroscopy .....	79
4.2 Speculation on improvements to the technology.....	80
<b>5.0 CONCLUSIONS .....</b>	<b>81</b>
5.1 Synthesis of conclusions in chapter 2, 3 and 4.....	81
5.2 Recommendations for future work.....	82
<b>BIBLIOGRAPHY .....</b>	<b>85</b>
<b>BIOGRAPHICAL NOTE .....</b>	<b>88</b>

## Table of Figures

Figure 1: Formation of aluminum spikes in a silicon substrate leading to short-circuiting and device failure. ....	12
Figure 2: Schematic of the process flow for producing ultra-high purity titanium. ....	14
Figure 3: Molten salt electrorefining cell.....	15
Figure 4: Redox looping in electrorefining and the chemical short circuit .....	16
Figure 5: Schematic illustration of waveform for linear sweep cyclic voltammetry.....	20
Figure 6: Schematic illustration of the waveform for ac voltammetry.....	22
Figure 7: Schematic illustration of a 30° phase shift between the ac potential and ac current.....	23
Figure 8: Relationship between the phase angle and (a) impedance in the vector plane, and (b) the current and potential phasors. ....	23
Figure 9: Linear sweep cyclic voltammogram for 267 mM $K_2TiCl_6$ in CsCl-NaCl-KCl	24
Figure 10: Determination of reduction potentials for the chlorotitanates...data from Chassaing, Basile & Lorthioir 1979.....	29
Figure 11: Ternary phase diagram for CsCl-NaCl-KCl. Copied from Phase Diagrams for Ceramists, 1969 Supplement. Based on Il'yasov & Bergman, 1962.....	31
Figure 12: Electroanalytical cell .....	33
Figure 13: ac voltammogram of supporting electrolyte; CsCl-NaCl-KCl; 693°C; WE=GC, CE= $C_{graph}$ , RE=Ag/Ag <sup>+</sup> ; $v=10$ mV/s; $\Delta E=5$ mV; $\omega/2\pi=100$ Hz. ....	37
Figure 14: ac voltammogram of 267 mM $K_2TiCl_6$ in CsCl-NaCl-KCl; 730°C; WE=GC, CE= $C_{graph}$ , RE=Ag/Ag <sup>+</sup> ; $v=10$ mV/s; $\Delta E=20$ mV; $\omega/2\pi=100$ Hz.....	39
Figure 15: ac voltammogram of 254 mM $K_3TiCl_6$ in CsCl-NaCl-KCl; 730°C; WE=GC, CE= $C_{graph}$ , RE=Ag/Ag <sup>+</sup> ; $v=10$ mV/s; $\Delta E=20$ mV; $\omega/2\pi=100$ Hz.....	40
Figure 16: Variation of phase angle with dc potential. ....	41
Figure 17: Schematic of the variation of the symmetry of the energy barrier for different values of the transfer coefficient. From Bard & Faulkner, 1980, p.97. ....	45
Figure 18: Effect of the transfer coefficient on the symmetry of the current-overpotential curves. Notice that -50 mV produces "a" current response which is almost 3 times "b" which is the current response for +50 mV. From Bard & Faulkner, p.104.....	47
Figure 19: $\cot\phi$ vs $\omega^{1/2}$ for $Ti^{3+}/Ti^{2+}$ .....	49
Figure 20: $\cot\phi$ vs $\omega^{1/2}$ for $Ti^{2+}/Ti^0$ .....	50
Figure 21: Schematic representation of spectroscopic methods.....	53
Figure 22: Stokes Raman spectrum of $\beta-TiCl_3$ at room temperature. From Fraser, et al, 1977.....	55
Figure 23: Absorption spectra for 32.3 milli-molal $TiCl_3$ in LiCl-KCl at various temperatures. From Sørliie and Øye, 1981.....	57
Figure 24: Absorption spectra for 20.1 milli-molal $TiCl_2$ in LiCl-KCl eutectic at various temperatures. Sørliie and Øye, 1981 .....	58
Figure 25: Fiber optic interface system and the standard spectrographic set-up for absorption experiments. ....	61
Figure 26: Fused quartz spectroscopic cell.....	62
Figure 27: Raman spectrum of $K_2TiCl_6$ in KCl at 25°C (solid).....	63
Figure 28: Expanded view of above. Notice the two high energy peaks.....	64
Figure 29: $TiCl_3$ Solid Raman spectrum.....	65

Figure 30: $K_2TiCl_6$ 287 mM in CsCl-NaCl-KCl at 660°C.....	65
Figure 31: Absorption spectrum for $Ti^{3+}$ , 330 mM in CsCl-NaCl-KCl, temperature as indicated. ....	67
Figure 32: Absorption spectrum of $TiCl_3$ at varying concentrations. Temperature was constant at 688°C.....	68
Figure 33: Absorption spectrum for $TiCl_3$ at various concentrations. Recorded using a fiber optic collection system .....	69
Figure 34: Absorption spectrum of $TiCl_2$ added to $TiCl_3$ in the eutectic electrolyte. Ratios vary from $Ti^{3+}$ only to 6:1 $TiCl_3$ to $TiCl_2$ (intermediate ratios were 50:1, 30:1, 20:1, 8:1, 7:1). ....	70
Figure 35: Concentration calibration curve for absorption peak at 12,700 $cm^{-1}$ . Temperature is 688°C.....	72
Figure 36: Calibration curve for the absorption peak at 6000 $cm^{-1}$ . Dotted line is the trendline calculated for the data using the origin as an intercept. Temperature is 688°C.....	73
Figure 37: Peak ratio of the 12,700 $cm^{-1}$ band to the 6,000 $cm^{-1}$ band for the various ratios of $Ti^{3+}$ and $Ti^{2+}$ . Temperature is 688°C.....	75
Figure 38: Peak height ratio for 12,700 $cm^{-1}$ and 6,000 $cm^{-1}$ at various ratios of $Ti^{3+}$ and $Ti^{2+}$ . Temperature is 580°C.....	76

## Acknowledgements

I am indebted to numerous people who have contributed to my doctoral education in general and this work in particular. I would like to thank:

Professor Donald Sadoway, my thesis advisor, and so much more. We have worked together so well on seeing his vision for this project become my vision and then a reality. A mentor in every sense of the word and an educator to the core.

The members of my thesis committee — Professor Ronald Latanision, Professor Sandra Burkett, and Dr. Sheng Dai for their insights and assistance at various points during the work and especially in preparing the final document.

Honeywell, The ALTA Group, my sponsor, for full financial support of the project and graduate education. The frequent site visits have clarified the industrial need and highlighted areas for improvement time and again.

Oak Ridge National Laboratory for serving as my research lab away from home for the spectroscopic parts of the investigation. In particular, I would like to thank again Dr. Sheng Dai for hosting me on five different occasions and making his laboratory facilities fully available as well as his personal analytical expertise. Mark Burleigh for being an exquisite host each time I was in Tennessee. Haiming Xiao for his assistance with the high temperature Raman studies. Michael Lance, at the High Temperature Materials Laboratory at ORNL, for his assistance with the solid Raman spectra.

Hongmin Zhu for his molten salt and electrochemical expertise. His insights have been invaluable and the practical help with experimentation and developing the lab's competency in ac methods were critical to the work. Additionally, the extraordinary glass-blowing expertise and experimental design contributions were key to the success of the work.

Guenter Arndt for his countless hours of consulting on experimental apparatus design and for his golden hands in executing those designs.

My group members, past and present, who have put up with my quirks and always been there for fun and help: Minoru Nakajima, Steen Nissen, Biying Huang, Hongmin Zhu, Michael Joerger, Ali Amini, Patrick Trapa, & Simon Mui.

The great MIT undergraduates who worked on UROP's with me: Danny Lai and Ashley Salomon.



The Graduate Student Council for providing a great education and supporting me over the last year when various duties called. This group of people has been there for me and the graduate student body and I am just lucky to have worked with them.

Finally, to my family and friends who have always had faith in me. Especially, roommate Brian Schuler and close friends Adam Cotner and Anand Raghunathan. Classmates in 1996, friends forever!

MIT provides a unique flavor of education. I have had an opportunity to taste many of the different flavors and would like to feel that I have contributed some of my own. I would like to thank all those at MIT who have come before me and will continue after...you make this place great.

## **1.0 Introduction**

### **1.1 BACKGROUND**

#### *Titanium metallurgy*

Since the 1950's, titanium has been known as the space age metal due to its prominence in high performance applications for the aerospace industry. Titanium is the fourth most abundant element in the earth's crust and has an attractive combination of characteristics in both its pure and alloyed forms. Its excellent strength-to-weight ratio is supplemented by its resistance to corrosion and high temperature stability. This combination leads to various applications in the marine, chemical, and medical industries in addition to the well known aerospace applications.

In spite of its abundance, titanium extraction produces an expensive final product (at the time of this writing, titanium alloy prices per pound are three times that of aluminum and ten times that of mild steel). (MetalPrices.Com, 2000) The first step in titanium extraction is the carbonylation of titanium ore ( $\text{TiO}_2$ ) to produce titanium tetrachloride ( $\text{TiCl}_4$ ), which is purified through fractional distillation.  $\text{TiCl}_4$ , often called "tickle", is then metallothermally reduced with sodium (Hunter process) or magnesium (Kroll process) to produce commercially pure, porous titanium metal called "sponge." Further cleaning and crushing prepares the metal for the

complicated melting techniques (vacuum-arc remelting or electron beam melting) needed to produce metallurgical grade titanium ingot.

### *Commercial significance of high purity titanium*

The microelectronics and semiconductor manufacturing industries produce a number of products which require deposition of high purity materials (microprocessors, DRAM, etc.). One way that these materials are transferred to the silicon wafer is a physical vapor deposition (PVD) process called sputtering. In this process, the deposition surfaces of the silicon wafers and the source targets are placed opposite one another in a controlled atmosphere sputtering machine. Using a system of magnets behind the sputtering target, a plasma is focused onto the source material surface. Depending on the actual system employed, the beam is rastered (usually in a ring pattern) across the surface of the target and atoms are sputtered from the source. These atoms travel to the deposition surface based on a path related to the processing conditions and the nature of the source and deposition surfaces. There are a number of key characteristics of the sputtering target which affect the quality of the deposition and the subsequent performance of the device produced. Of these characteristics, purity (metals and gases) is of extreme importance and is a criterion by which products can be differentiated in the marketplace.



*From commercially pure to ultra-high purity*

Molten salt electrolysis as a technique for metal production holds many advantages over pyrometallurgical methods. This advantage is derived from the high ionic conductivities of the melts (which allow substantial currents with modest potential drops), high diffusivities of highly soluble electroactive species (which eliminate concentration polarization), low activation polarization and viscosities, as well as few competing reactions. The most significant drawbacks to molten salt electrolysis are mainly tied to its high temperature nature: highly corrosive melts, high vapor pressure of the salts employed, and the low electromotive selectivity experienced for a number of melts. (Driscoll, 1991) Furthermore, many of the processes suffer from low current efficiencies because of redox looping that occurs if multiple valence states are available for the metal ion being electrorefined. Unfortunately, most metals do form subvalent species so these parasitic redox reactions are consistently troublesome.

Aluminum, magnesium, sodium, lithium, and potassium are the metals that are produced primarily by fused salt electrolysis. The decision to use a molten salt electrolyte is not one made lightly. The engineering issues related to the high operating temperatures and corrosive environments are not trivial. As such, molten salt electrolysis is usually employed when the deposition potentials in aqueous electrolytes are too extreme (more negative than the potential for hydrogen gas evolution) or when water is not an appropriate

solvent. Molten chloride electrolysis is only used to meet high purity requirements in titanium production with a large percentage of titanium metal production coming from the metallothermic reduction of  $TiCl_4$  described above.

### *ALTA flow process*

Founded in 1986, the ALTA Group, a fully owned subsidiary of Honeywell, Inc., is a leading supplier of high purity sputtering materials to the microelectronics industry. ALTA produces its own commercially pure titanium sponge in Salt Lake City, UT and then electrorefines the sponge in Fombell, PA using a fused salt technology. Subsequent cleaning and electron beam remelting of the crystal (electrorefined titanium) produce the high purity ingot from which the titanium target blanks are manufactured and prepared for shipment. The as-shipped target has been formed to allow direct insertion into process sputtering machines at the microelectronic fabrication centers.

This flow process is shown schematically in Figure 2.

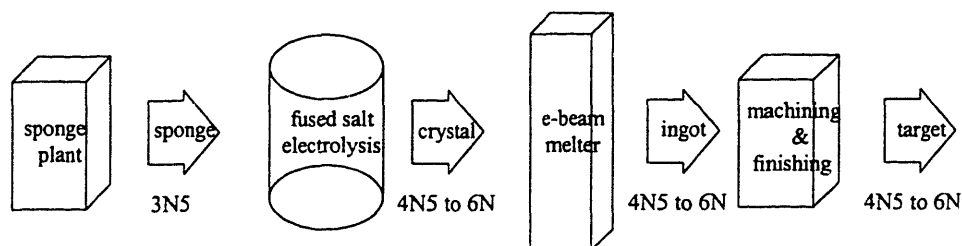


**Figure 2: Schematic of the process flow for producing ultra-high purity titanium. 3N5 is 99.95% pure, 4N5 is 99.995%, etc.**

*Existing methods for tracking process chemistry*

The electrorefining process employs an electrolyte composed of equimolar KCl-NaCl with low weight percent  $\text{TiCl}_2$  (5 to 10 wt%). Titanium sponge is fed into a pot which is anodically polarized and ultra pure titanium is employed as a central cathode as shown in Figure 3. The anode is the source of the divalent titanium and the cathode is the collection point for the product (a dendritic metal called “crystal”, the christmas tree-like morphology of which is evidence of a diffusion limited process). The cell is run at constant current. The oxidizing potential established at the anode causes titanium to dissolve by converting it from a neutral species to the divalent ion which is soluble in the

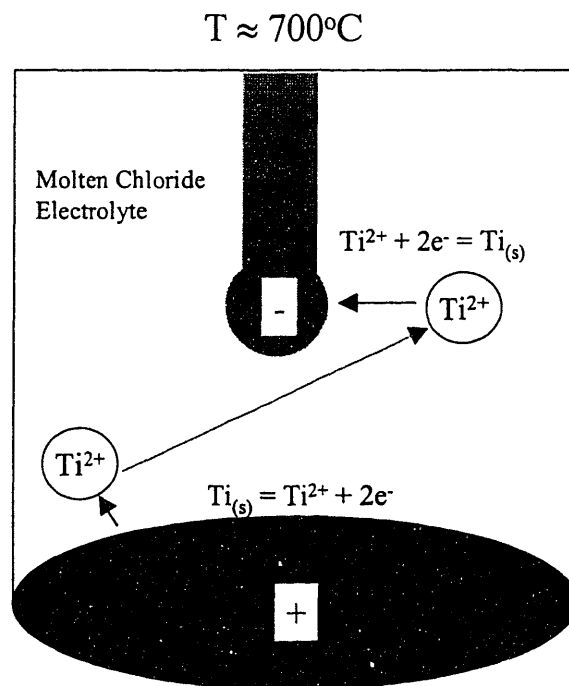


**Figure 3: Molten salt electrorefining cell.**

electrolyte. At the cathode, the divalent titanium species then accepts two electrons to become neutral titanium, which crystallizes on the electrode. The refining mechanism is determined by the potentials at the anode and cathode. In a molten chloride bath, the potential at the anode is not sufficiently extreme for impurities such as iron, copper, nickel, and chromium to dissolve, whereas the cathodic potential for titanium deposition is sufficiently low such that zirconium, barium, and calcium are not deposited once they enter the bath. Currently, the composition of the fused salt electrorefining bath is only investigated via *ex situ* wet chemistry methods and is reported as the average electronic valence (AEV) of titanium.

Because of the aliovalent nature of the chlorotitanate systems, an electrorefining process is prone to low current efficiencies due to parasitic side reactions. These side reactions are shown schematically in Figure 4.

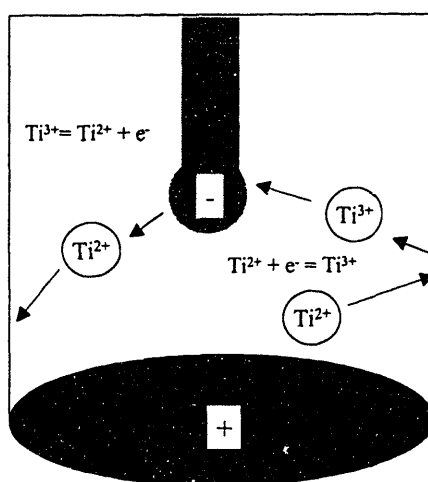


**Figure 4: Redox looping in electrorefining and the chemical short circuit**



Redox looping occurs when divalent titanium is oxidized at the anode and the resulting trivalent titanium is subsequently reduced at the cathode. This reaction allows for electrochemical "short-circuiting" whereby the current passed through the cell is not used solely for metal dissolution and production. This redox looping is hard to eliminate because of the thermodynamic stability of the trivalent titanium species (see Section 2.3, Physical Chemistry). However, years of experience have shown that a certain ratio (AEV~2.1) of chlorotitanate species produces the best crystal. (Haarberg, 1993) The justification for this observed correlation is not understood, and there are no reports of attempts at *in situ* verification.

## **1.2 SCOPE OF THE PRESENT STUDY**

The goal of the present investigation was to gain a better understanding of the science underlying the molten salt electrorefining process for production of high purity titanium. However, although the industrial process has been well engineered, empiricism is the justification for much of the current industrial practice. As competition in the market for supplying high purity titanium intensifies, the inefficiencies of the process become major costs and, if not well understood, could be hard to control and impossible to reduce. Knowing the underlying science of the fused salt electrorefining is thus a critical step in establishing and executing the most efficient production process for ultra-high purity titanium sputtering targets.

There are three parts to the question:

- Interfacial phenomena (multiple reduction steps and the kinetics associated with each) related to the faradaic process ... investigated with electroanalytical techniques,
- Bulk chemistry of the electrolyte (structure of the chlorotitanate complexes) that describes the nature of the species present during the electrorefining process ... investigated with spectroscopic techniques;
- Recommendations for on-line control or possible sensor technologies to improve operating practices.

### **1.3 ORGANIZATION**

The thesis is organized to describe the characterization of the chlorotitanate melts. Chapter Two presents the investigation of the electrochemical behavior of the melts. Chapter Three presents the spectroscopic investigation of the melts, with a particular focus on the UV/visible absorption techniques. Chapter Four provides a discussion of the possible technologies that could be used industrially as on-line controls as well as providing suggestions for improvements to the current practice. The concluding chapter provides recommendations for future work and summarizes the contributions of the thesis to the understanding of the behavior of the molten chlorotitanates.

## 2.0 Electroanalytical Chemistry

### 2.1 SUMMARY

Electroanalytical investigation of the chlorotitanate melts has produced a better understanding of the nature of the electrode reactions. By looking at the multiple reduction steps and the kinetics associated with each step:

- for the first time, phase angle information from ac voltammetry has been used to quantitatively determine kinetic parameters for the molten chlorotitanates: at a glassy carbon electrode the transfer coefficient ( $\alpha$ ) and the standard rate constant ( $k^\circ$ ) have been determined; and
- the metal production step ( $\text{Ti}^{2+}/\text{Ti}^0$ ) has been determined to be the slow step in the electrorefining process.

### 2.2 BACKGROUND

The study of electrochemical reactions is largely a study of interfacial phenomena. The driving force for these reactions is the electrochemical potential. This potential can either be generated internally or dependent on an external source of electrons. In the present study the response of the system to applied potential under various dynamic situations has been investigated.

The most common electroanalytical technique employed to study a faradaic process is linear sweep voltammetry (LSV). In LSV, the potential of a chosen electrode, termed the working electrode (WE), is controlled with respect to a reference electrode so as to vary linearly with time. The current

flow between the WE and a counter electrode (CE) is measured. In cyclic voltammetry (CV), the potential sweep is reversed at a value termed the switching potential and typically returned to its initial value. The plot of current versus potential is known as a voltammogram and is representative of the current-potential characteristic of the WE. A schematic representation of one cycle in a LSV is shown in Figure 5.

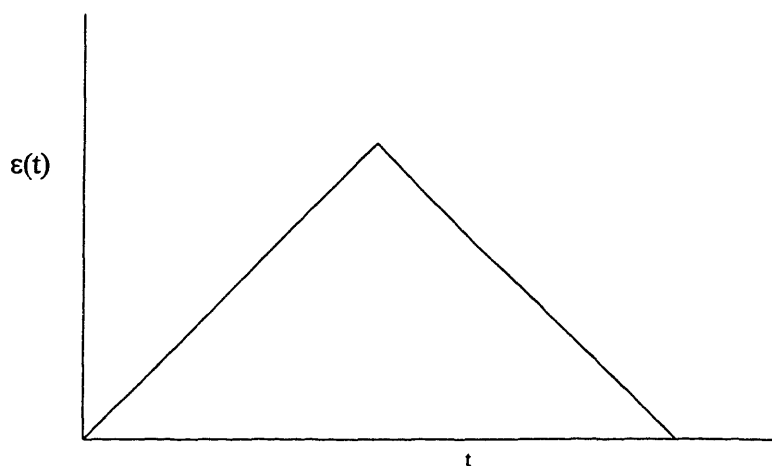


**Figure 5: Schematic illustration of waveform for linear sweep cyclic voltammetry**

The variables that can be adjusted are the sweep rate (i.e., the slope of the linear scan) and the potential range. This technique has been employed in numerous electrolytes and in various experimental arrangements. The technique is especially well suited to investigating the reaction steps for faradaic processes and determining reduction potentials as well as the number of electrons exchanged. However, in high temperature molten salt

investigations, it is much more difficult for the technique to provide meaningful data due to the high background current caused by the effects of convection and the high energy due to the absolute temperature.

In addition, the current response is somewhat difficult to interpret due to the charging currents that develop in response to a rapid change in the electron population on the electrode. As a matter of fact, at high sweep rates the charging current ( $i_{\text{charge}}$ ) can be many times larger than the faradaic current ( $i_{\text{faradaic}}$ ). This is problematic because the purpose is to study the faradaic process, yet the signal that is recorded has much of its value related to the non-faradaic process of charging the double layer at the electrode/electrolyte interface. In order to minimize these charging currents, low sweep rates are employed, which keep  $dE/dt$  as low as possible.

Low sweep rates help dc voltammetric studies to avoid the deleterious influence of charging currents, but at the expense of the kinetic information that can be elicited. The trend in recent years has been to employ ac methods such as ac voltammetry to gain access to kinetic information about faradaic processes. This technique uses a voltage waveform consisting of an ac ripple superimposed on a dc ramp. Figure 6 shows a schematic representation of this voltage waveform.

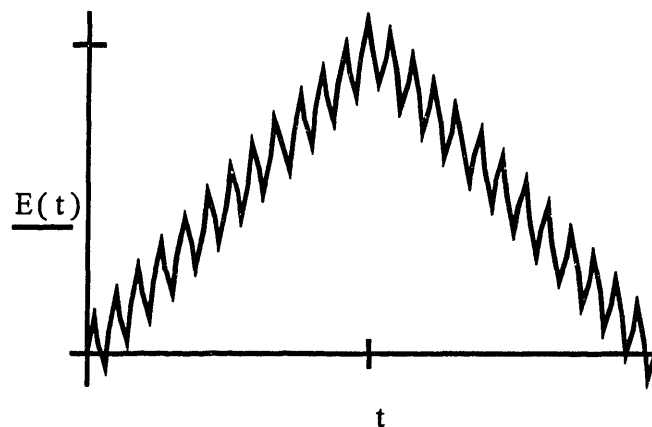


**Figure 6: Schematic illustration of the waveform for ac voltammetry**

The data collected from such an experiment include the ac current response as well as the phase angle between the potential (stimulus) and the current (response). The value of the phase shift can vary from 0 degrees (in phase) to 90 degrees (completely out of phase) depending on the nature of the electrical load as measured by the potentiostat. Purely resistive loads do not cause phase shifts, while reactive loads (capacitive or inductive) do. An intermediate phase shift is depicted in Figure 7. In practice, one determines phase angle from the measurement of the instantaneous impedance, which has imaginary and real components. These can be viewed as components of a vector. Alternately, the phase angle is the angle between the current and voltage vectors. By convention, the current vector is positioned on the real axis. Figure 8 shows the vector plane and indicates the conventions for measuring the phase angle.

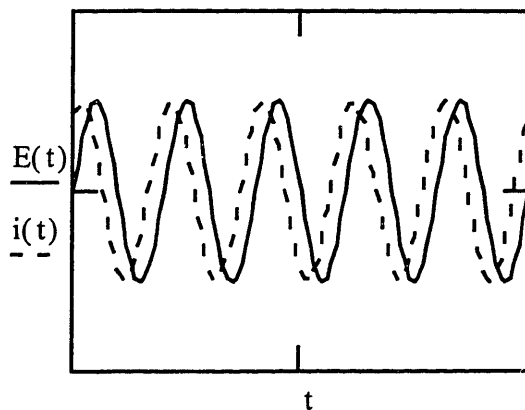


**Figure 7: Schematic illustration of a 30° phase shift between the ac potential and ac current.**

AC voltammetry is attractive for additional reasons relevant to the nature of the system under study. LSV is an attractive and effective technique for characterizing faradaic processes. It is most effective in aqueous systems

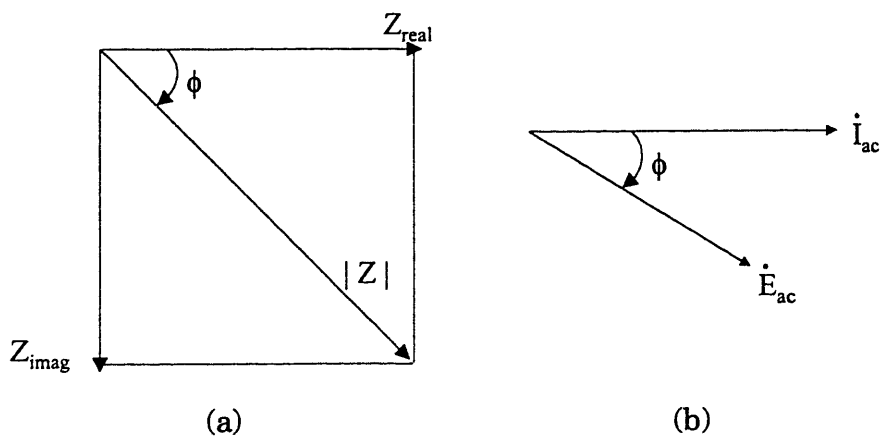


**Figure 8: Relationship between the phase angle and (a) impedance in the vector plane, and (b) the current and potential phasors.**

(although molten salt studies do exist) because in high temperature systems the influence of thermal noise and convection currents is substantial.

Determination of the proper baseline for analytical work is a bit of an art, and the opportunity for ambiguity increases. A better than average CV for the high temperature chlorotitanate system is shown in Figure 9. It is possible to discern from this voltammogram an estimate of the potentials on the forward scan, but the reverse scan has significant peak separation which leads to ambiguity as to the proper peak assignments. There are different numbers of forward and reverse peaks, and it is difficult to determine which of the

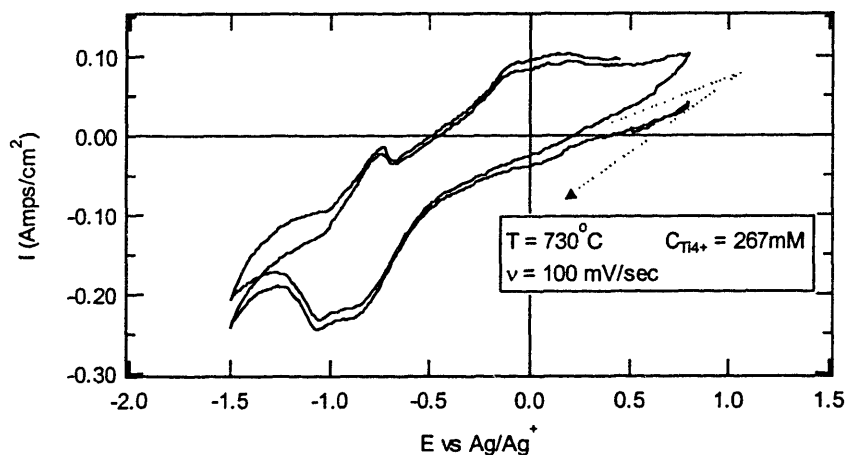


**Figure 9: Linear sweep cyclic voltammogram for 267 mM  $K_2TiCl_6$  in CsCl-NaCl-KCl**

forward peaks are correlated to which reverse peaks. Additionally, it is difficult to discern reduction peaks at the potentials near 0 V (vs. Ag/Ag<sup>+</sup>). Establishment of a baseline for quantitative analysis is difficult, and inherent to the technique is the lack of a direct route to kinetic information. In this



molten salt system, ac methods appear to be more effective for investigating the kinetics of the faradaic processes. Surprisingly, there are very few reports in the literature of studies in which ac methods have been used in the investigation of molten salt systems. In particular, there are no reported ac studies of the molten chlorotitanates.

The rest of this chapter is organized into five sections. Section Two reviews the electroanalytical literature with a focus on molten salts and especially the molten chlorides and titanium studies. Section Three describes the apparatuses and procedures and Section Four introduces typical results. These results are discussed in the 5<sup>th</sup> Section and the method by which they were used to calculate kinetic information about the faradaic processes occurring in the cell is described. The final section summarizes the experimental findings and offers general conclusions about the electroanalytical work.

### **2.3 EARLIER WORK**

#### *Electrochemistry*

A selective review of the anodic and cathodic processes associated with the molten salt electrolysis of titanium has been presented previously. (Girginov, 1995) Through examination of the last twenty years of work, the general methods and kinetics of electrodeposition of refractory metals have been compiled. However, this review can be misleading since the results of

these studies have been presented without critical evaluation and contradictions are presented without comment. The review does point out the absence of an understanding of the anodic and cathodic electrode reactions for the titanium electrorefining process and recognizes that the database of kinetic information is poor.

### *Physical Chemistry*

Differential thermal analysis has been employed to identify the extent of complexation for the trivalent and tetravalent chlorotitanate systems in alkali chloride melts. As a result, three different complexes have been identified for the trivalent systems ( $\text{TiCl}_6^{3-}$ ,  $\text{Ti}_2\text{Cl}_9^{3-}$ , and  $\text{TiCl}_4^-$ ) (Korol'kov, 1968; Chassaing, 1979b), as well as one tetravalent titanium complex ( $\text{TiCl}_6^{2-}$ ) (Morozov, 1960; Flengas, 1960a; Lister, 1963) in equilibrium with dissolved  $\text{TiCl}_{4(g)}$ . (Smirnov, 1966) In addition, numerous thermodynamic studies of the electromotive forces of transition metal chlorides in equimolar NaCl-KCl have been reported. (Flengas, 1957a; Flengas, 1957b; Flengas, 1958a; Flengas, 1958b; Flengas, 1959; Tumidajski, 1991)

Further study of the system indicates that the presence of titanium metal and trivalent titanium in the same system requires that divalent titanium be present. The equilibrium ratio between the trivalent and divalent titanium has been reported as 1:9 (Flengas, 1960) which is similar to the ratio that would be necessary to produce an AEV of 2.1. Further, this work indicates that the experimental requirement that investigation of trivalent

titanium in solution without divalent titanium is not possible when titanium metal is present in the same system.

*Sweep potential experiments with questionable electrodes*

Much of the previous work on the electrochemistry of the chlorotitanates suffers from basic experimental deficiencies. These include: poor selection of reference systems (Menzies, 1959/60; Baboian, 1965; Popov, 1991), use of working electrodes that are not inert (Reid, 1961), or employment of geometries in which linear, one-dimensional diffusion can not be assumed. (Haarberg, 1993)

*Titanium reduction pathways in different electrolytes*

Because of the questionable nature of the electrode systems employed, the reduction potentials reported in the literature are often unreliable. However, analysis of reduction pathways provides important information about the expected behavior of the chlorotitanate systems under study. In chloride baths, it has been repeatedly reported that the reduction pathway proceeds from the tetravalent species through the trivalent and divalent states before undergoing a two electron step to deposit neutral metal. (Haarberg, 1993; Baboian, 1965; Popov, 1991) These results are further supported by reports of the reduction pathway from studies with better control of the electrode systems. (Flengas, 1960b; Nardin, 1977; Chassaing, 1979a; Oki, 1987; Ferry, 1987) Electrochemical reduction of titanium in fluoride melts has been studied, with the reported result that the trivalent state is stabilized in

these melts and metal deposition occurs due to a process involving the exchange of three electrons. (Wurm, 1957; Clayton, 1973; Sequeira, 1988)

*Recent electroanalytical studies of  $Ti^{3+}$  including ac methods*

To date, the best electroanalytical studies have been performed in France. The first study followed the effect of cationic radius of the supporting electrolyte (alkali chlorides) on the reduction behavior of the molten salt system. (Chassaing, 1981a) By examining the spectroscopic behavior of the melt as well as the electrochemical behavior, Chassaing et al. were able to report that as the cationic radius increases (from  $Li^+$  to  $Cs^+$ ),  $Ti^{2+}$  becomes less stable with respect to  $Ti^{4+}$  and  $Ti^{3+}$ . Stepped current and potential experiments were also employed to investigate the reversibility of the  $Ti^{3+}/Ti^{4+}$  and  $Ti^{3+}/Ti^{2+}$  couples. (Ferry, 1987)

The half-wave potentials for the various reduction steps of  $Ti^{4+}$  to metal were determined by LSV at low sweep rates with a large working electrode. (Chassaing, 1979a) The supporting electrolyte was a LiCl-KCl eutectic with small addition of  $BaCl_2$ . The data from these experiments are shown in Figure 10.

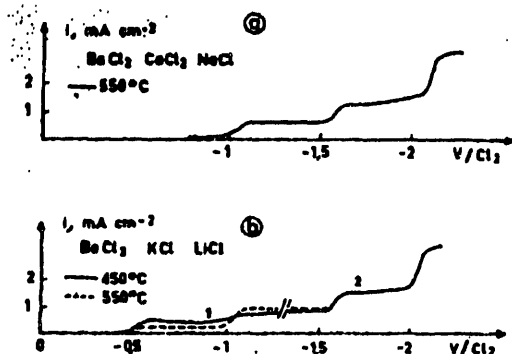


**Fig. 1. Reduction steps of  $TiCl_4$ . (a)  $BaCl_2-CaCl_2-NaCl$  (16:46.5:37.5 mol.%) eutectic,  $T = 550\text{ }^\circ\text{C}$ ; working electrode, vitreous carbon V 25;  $\nu = 200\text{ mV min}^{-1}$ . (b)  $BaCl_2-KCl-LiCl$  (6:40:54 mol.%) eutectic; —,  $T = 450\text{ }^\circ\text{C}$ ; - · - ·,  $T = 550\text{ }^\circ\text{C}$ ;  $\nu = 200\text{ mV min}^{-1}$ . Working electrode: 1, vitreous carbon V 25; 2, nickel.**

**Figure 10: Determination of reduction potentials for the chlorotitanates...data from Chassaing, Basile & Lorthioir 1979.**

The half-wave, or characteristic, potentials identified as a result of the experiments above are shown in the table below:

**Table 1: Characteristic potentials for titanium reduction steps in molten chlorides. Based on Chassaing, Basile & Lorthioir, 1979.**

$Ti^{4+}_{\text{complex}} + e^- \Rightarrow Ti^{3+}$	+0.25
$Ti^{4+}_{\text{gas}} + e^- \Rightarrow Ti^{3+}$	-0.20
$Ti^{3+} + e^- \Rightarrow Ti^{2+}$	-0.8
$Ti^{2+} + 2e^- \Rightarrow Ti^0_{(s)}$	-1.2

No literature has been located regarding the use of ac voltammetry techniques in high temperature molten salts. The technique has been

employed to study  $\text{Ti}^{4+}/\text{Ti}^{3+}$  in oxalic acid and acetone at room temperature. (Bard Chapter 9, 1980) However, investigations of the kinetic properties of faradaic processes using ac methods are few. Researchers have been trying to employ ac methods in high temperature systems, but the use of the phase angle information for extracting kinetic determinations has been largely unsuccessful. (Petrushina, 2000)

## 2.4 EXPERIMENTAL/APPARATUS/TECHNIQUES

The electrochemical experiments were performed using a single experimental apparatus and a uniform technique. The supporting electrolyte (used as a solvent for the chlorotitanates as well as to reduce the migration currents to negligible values) was a eutectic mixture of cesium chloride, sodium chloride and potassium chloride. The ternary phase diagram is shown in Figure 11. Based on the phase diagram, the eutectic composition was determined to be 47 mol % CsCl, 26 mol % NaCl and 27 mol % KCl (70:13:17 respectively on a weight percent basis). These three chlorides are widely available commercially. They were weighed and mixed in open air, placed in either a fused quartz crucible or an alumina crucible that was made airtight and then placed in a furnace where the mixture was melted. The pre-melted

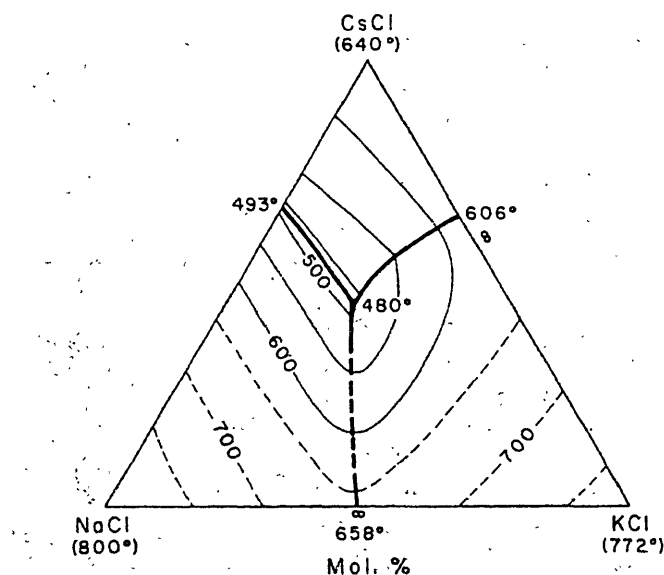


**Figure 11: Ternary phase diagram for CsCl-NaCl-KCl. Copied from Phase Diagrams for Ceramists, 1969 Supplement. Based on Ilyasov & Bergman, 1962.**

eutectic salt was transferred to an argon filled dry box where the salt was crushed and stored until use.

The chlorides of titanium are somewhat unstable and react with moisture in the air. Titanium trichloride and dichloride were obtained in their pure form from Aldrich. The trichloride was the alpha form of the solid, deep violet in color, 99% purity, with <100 ppm H<sub>2</sub>O. The dichloride was a black solid, 99.98% purity, with <100 ppm H<sub>2</sub>O.

Titanium tetrachloride is a colorless liquid at room temperature and has a normal boiling point of 134°C. In this study, tetravalent titanium was introduced into the melts as the chlorotitanate, K<sub>2</sub>TiCl<sub>6</sub>, a solid complex with KCl obtained via the gas-solid reaction between TiCl<sub>4(g)</sub> and KCl<sub>(s)</sub>. This compound was prepared in the laboratory according to the two-zone reaction process described by Flengas. (1960a) The product of this process was flame-sealed in a glass ampoule and transferred to the glove box for storage.



The experimental apparatus is shown in Figure 12. This is a three

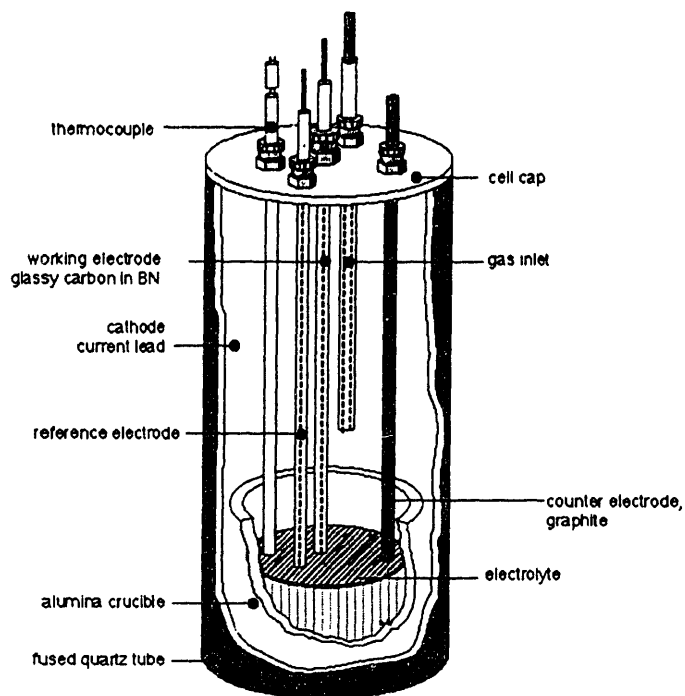


**Figure 12: Electroanalytical cell**

electrode arrangement with a central working electrode, a large-area counter electrode, and a reference electrode. Additionally, two ports were included in the cap to accommodate a thermocouple well and a gas flow tube. The thermocouple well was constructed from a closed-one end fused quartz tube and was lowered into the melt at the same depth as the working electrode.

The crucible for the experiments was a right circular cylinder of alumina, 40 mm in diameter.

Numerous working electrodes were employed, but the most reproducible results were obtained using the inert glassy carbon electrode. A glassy carbon rod (2 mm in diameter) was sheathed in boron nitride to provide a flat micro-electrode and to insure that the one-dimensional linear diffusion assumption is accurate. The electrode surface was polished before each experiment in order to produce a clean and controlled surface.

A silver/silver chloride reference electrode was employed. All voltages reported in this work are relative to the  $\text{Ag}/\text{Ag}^+$  couple, which has a potential shift of -0.835 V versus the standard chlorine reference electrode at 1000K (-0.905 V at 723K). The reference electrode was constructed in this laboratory using a ¼" diameter closed-one-end mullite tube as the encasing. The closed end was ground with a polishing wheel so that its thickness was approximately one millimeter. The salt was prepared by melting a mixture of equimolar sodium chloride and potassium chloride with 5 mol % silver chloride. This mixture was melted, sealed and transferred to the dry box where it was crushed and stored. A Pyrex top was constructed in the lab to fit the top of the mullite tube as well as allowing a two millimeter silver wire to pass through. The silver wire was placed in the mullite tube, extending from the closed end through the glass cap. The cap was sealed with epoxy at the junction with the mullite tube as well as at the silver wire. This was allowed to cure overnight

before the apparatus was placed in the dry box. Once in the dry box, the pre-melted and crushed salt was added to the tube through a side tube in the glass cap. Once the crushed salt was inserted, the tube was made airtight and then removed from the dry box whereupon the side tube was immediately flame sealed. Numerous electrodes were prepared in this manner and typically would last for at least six months to a year. The typical failure mode was mechanical failure either in the body or the glass cap. There was no noticeable degradation in the electrochemical stability or performance of the electrodes over the time of their use. When not in use, the reference electrodes were stored in the dry box after being washed with de-ionized water and dried in an oven.

The cell was assembled outside the glove box with everything but the salt in the crucible. The entire assembly was then transferred into the dry box, partially disassembled to remove the crucible, and then reconstructed once the crucible had been filled with the eutectic salt and the appropriate chlorotitanate species. The assembly was then sealed and all valves were closed while it was removed from the dry box. The apparatus was positioned with the crucible in the hot zone of the furnace and the cap outside the furnace and shielded from as much of the heat as possible. The cell was then evacuated and backfilled with argon a few times before the furnace was started. The furnace temperature was raised to between 200° and 300°C while the final evacuation was performed. Once the temperature was stabilized at

300°C, the vacuum pump was removed from the system and the pressure was returned to atmospheric pressure by addition of argon. The system was then closed while the furnace was raised to the operating temperature. The pressure was vented if necessary, but otherwise the system remained closed for the duration of the experiment.

The electroanalytical experiments were performed through the exclusive use of Solartron electrochemical instrumentation. A Solartron 1286 potentiostat was used in combination with a Solartron 1260 frequency response analyzer to carry out the ac voltammetry described above. The instruments were connected to computer control software through an IEEE general purpose information bus (GPIB) board. The CorrWare<sup>®</sup> software program was used to control the 1286 for dc experimentation while ZPlot<sup>®</sup> software was used to control both the 1286 and 1260 for ac voltammetric experimentation.

## 2.5 RESULTS

The supporting electrolyte (in the present case the CsCl-NaCl-KCl eutectic) was chosen to allow the widest range of useful potential for the solutes of interest — in the present study  $Ti^{4+}$ ,  $Ti^{3+}$ , and  $Ti^{2+}$ . Figure 13 shows the ac current response of the supporting electrolyte. The potential was set initially at the rest potential (near 0 V vs. Ag/Ag<sup>+</sup>) and was swept first anodically and then cathodically at 10 mV/sec with a 5 mV peak-to-peak ac perturbation at 100 Hz. The anodic sweep was halted at +1.0 V as the

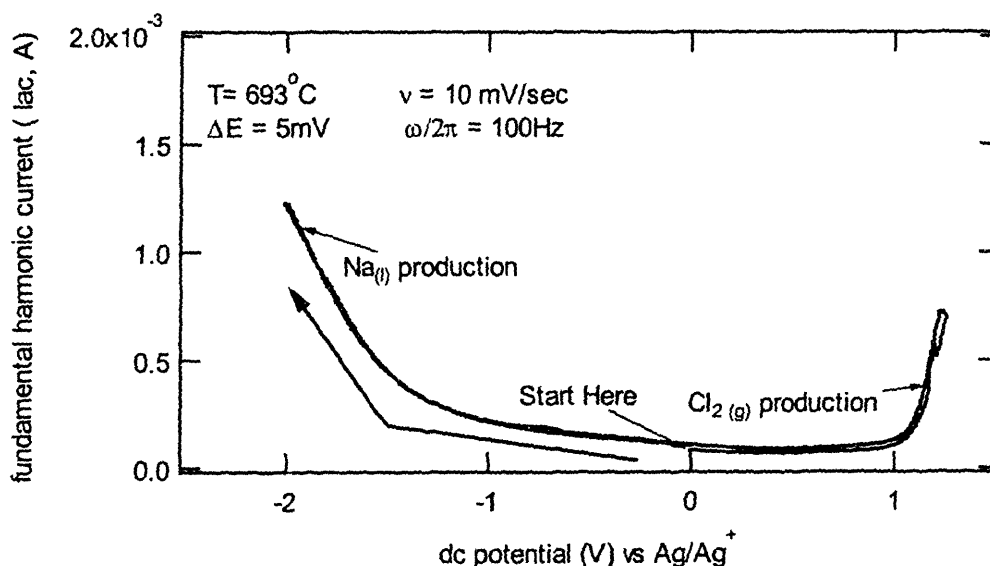
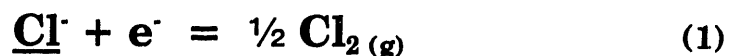


Figure 13: ac voltammogram of supporting electrolyte; CsCl-NaCl-KCl; 693°C; WE=GC, CE=C<sub>graph</sub>, RE=Ag/Ag<sup>+</sup>; v = 10 mV/s; ΔE = 5 mV; ω/2π = 100 Hz.

electrolyte started to break down due to the conversion of chloride ions to chlorine gas according to the reaction:



The sweep was then reversed and the cathodic sweep was continued to  $-2.0 \text{ V}$  where the electrolyte started to break down, this time due to the reduction of the alkali cations to their elemental form. The electrolyte breakdown reaction for the cathodic sweep was either:



or



or possibly both reactions. These data confirm that the supporting electrolyte has a suitably wide voltage window over which investigation of the chlorotitanates is feasible without the influence of electrolyte breakdown confusing the interpretation of the data.

Figure 14 shows the influence of adding an electroactive chlorotitanate species to the melt. In this case  $\text{Ti}^{4+}$  was added as  $\text{K}_2\text{TiCl}_6$  to the supporting electrolyte. Over the range of potential where the supporting electrolyte showed no current response, the addition of the  $\text{Ti}^{4+}$ -containing species causes considerable ac current response. At point A (+0.2 V) evidence of a reduction peak can be observed on the cathodic sweep. The current response then levels out before reaching a maximum again at a more cathodic potential, point B. The peak at point B is a very broad peak, but there is evidence of a high potential shoulder at B' that indicates a second faradaic process. Upon reversing the potential and sweeping in the anodic direction, the current trace

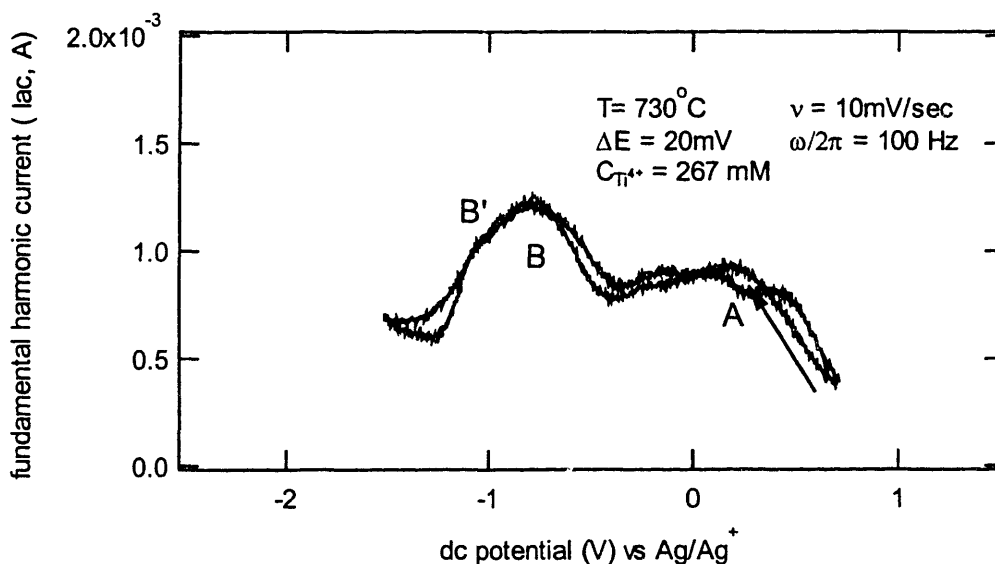


**Figure 14:** ac voltammogram of 267 mM  $\text{K}_2\text{TiCl}_6$  in  $\text{CsCl-NaCl-KCl}$ ; 730°C; WE=GC, CE=C<sub>graph</sub>, RE=Ag/Ag<sup>+</sup>; v= 10 mV/s; ΔE= 20 mV; ω/2π=100 Hz.

overlays the peak at point B and is split on the return through the potential

zone for peak A. This behavior was experienced over many different experiments with this particular trace being the most clear yet representative of the trend.

The behavior of the system upon addition of the trivalent chlorotitanate species is shown in Figure 15. In this case  $Ti^{3+}$  has been added as  $TiCl_3$  to the supporting electrolyte (where it subsequently forms a mix of the six-coordinate

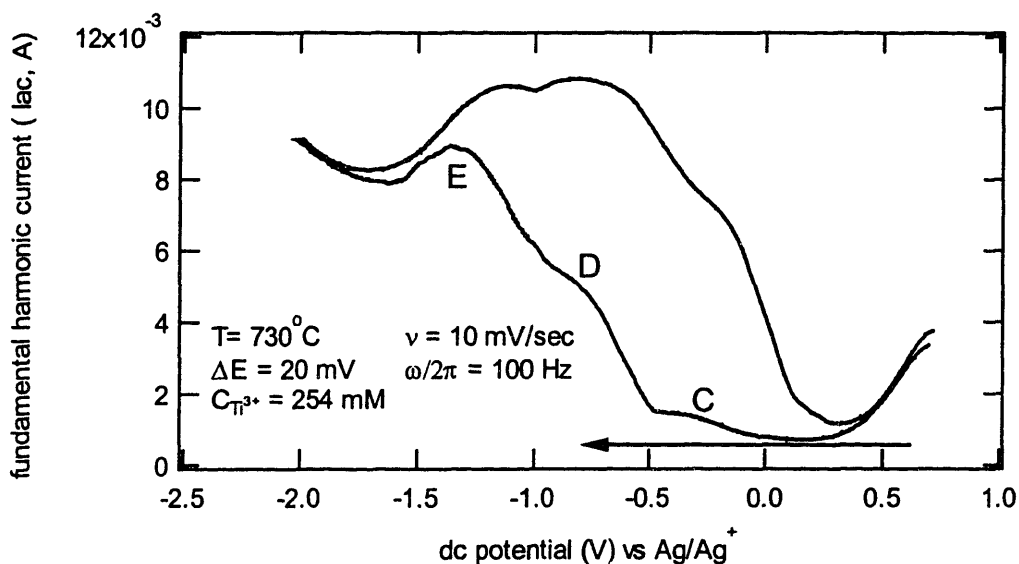


Figure 15: ac voltammogram of 254 mM  $K_3TiCl_6$  in CsCl-NaCl-KCl; 730°C; WE=GC, CE= $C_{graph}$ , RE= $Ag/Ag^+$ ;  $v = 10 \text{ mV/s}$ ;  $\Delta E = 20 \text{ mV}$ ;  $\omega/2\pi = 100 \text{ Hz}$ .

$K_3TiCl_6$  and the four-coordinate  $KTiCl_4$ , see Chapter 3). No  $Ti^{4+}$  was added and is presumed to be absent initially. Whereas in the previous sweep there was evidence of a faradaic process in the anodic potential regime, the associated peak was absent upon addition of only titanium trichloride. The first indication of a faradaic process is seen at point C (-0.2 V). At point D (-



0.8 V) evidence of the onset of a second faradaic process is seen. Finally, at point E (-1.2 V) the final faradaic reaction is seen before the potential is so extreme that the electrolyte breaks down via alkali metal production. The return sweep shows three peaks slightly offset from the characteristic (or half-wave) potentials measured on the forward sweep but still corresponding to the potentials at C, D & E.

For this same melt, Figure 16 shows the phase angle ( $\phi$ ) versus the dc potential for two different values of the frequency of the ac ripple with amplitude fixed at 20 mV. The peaks correspond to the characteristic potentials identified in previous figures (-0.20 V, -0.8 V and -1.2 V).

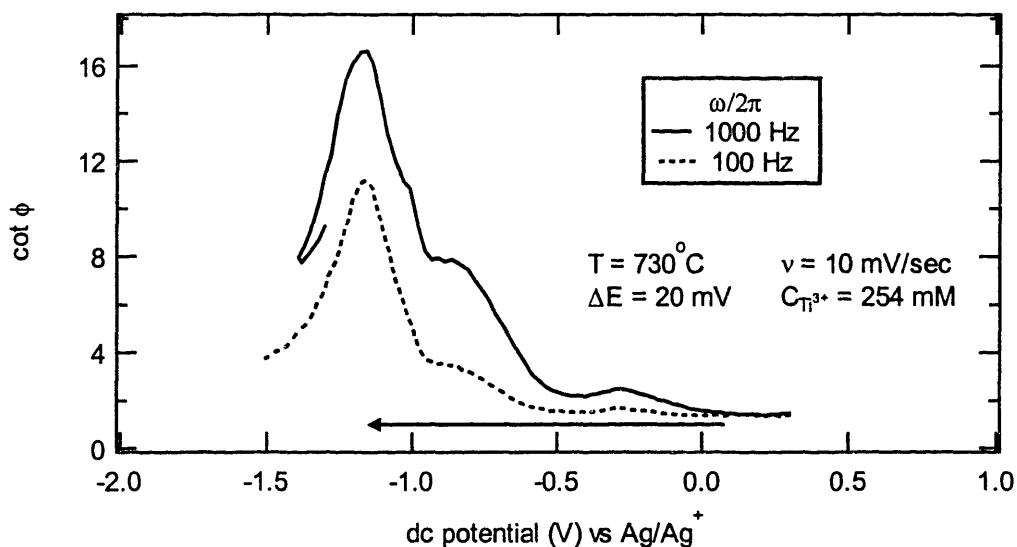


Figure 16: Variation of phase angle with dc potential.

## 2.6 DISCUSSION

The ac voltammograms (ACVs) presented in the previous section have characteristic potentials that correspond very well to the half wave potentials ( $E_{1/2}$ ) identified by Chassaing, Basile, & Lorthioir (CBL). The  $Ti^{4+}$  ACV shows peaks corresponding to the successive reduction of the chlorotitanate complex ( $TiCl_6^{2-}$ ) to a trivalent titanium species (+0.25 V), then to the divalent ion (-0.8 V) and then to metal (-1.2 V). This final peak is less easily discerned in the ACV for  $Ti^{4+}$  (a mere shoulder) but it is clearly evident in the  $Ti^{3+}$  ACV.

The  $Ti^{3+}$  ACV also provides confirmation of the gas reduction peak for  $Ti^{4+}$  (-0.2 V) which must have been generated as a result of the reverse sweep. The absence of the reduction peak for complexed  $Ti^{4+}$  (+0.25 V) is explained by the fact that there is no  $Ti^{4+}$  complex initially present in this melt. The data seem to indicate that the species generated on the reverse peak is a dissolved  $Ti^{4+}$  containing gas species as opposed to the complexed  $TiCl_6^{2-}$  observed when  $K_2TiCl_6$  is the electroactive species added to the melt.

The ability to detect the  $Ti^{4+}$  gas reduction peak in this melt is evidence of the high sensitivity of ac voltammetry. The prior work by CBL, who used dc methods only, showed evidence for this reduction peak at -0.2 V, but required that  $TiCl_{4,(gas)}$  be bubbled continuously at the working electrode. However, the ac technique allows detection at much lower concentrations due to the much shorter time scale of the measurement. Nevertheless, the characteristic

potentials agree between the two studies. Additionally, the relative ease of detection in ac voltammetry indicates another advantage of the technique: access to kinetic information.

AC voltammetry perturbs the system with minor fluctuations around a relatively low rate potential sweep. The ac current response carries important kinetic information about the faradaic reactions for which the characteristic potentials are also elucidated by the technique. This access to the kinetic information (as well as avoidance of the complicating influence of charging currents) is the reason that ac voltammetry was chosen for the present study.

Specifically, two important kinetic parameters are elucidated. First, the transfer coefficient,  $\alpha$ , indicates the asymmetry of the energy barrier between the oxidized and reduced species in a faradaic reaction. The transfer coefficient is accessible via the variation in phase angle with dc potential. The shift in potential of the maximum of  $\cot \phi$  from the half-wave potential ( $E_{1/2}$ ) allows determination of the transfer coefficient via the following relationship

$$E_{\cot\phi = \max} = E_{1/2} + \frac{RT}{nF} \ln\left(\frac{\alpha}{\beta}\right) \quad (4)$$

(all equations from Bard Chapter 9, 1980):

with

$$\beta = 1 - \alpha \quad (5)$$

which upon substitution for  $\beta$  and rearranging produces:

$$\frac{\alpha}{1-\alpha} = \exp\left(\frac{nF\Delta E}{RT}\right) \quad (6)$$

where

$$\Delta E = E_{\cot\phi = \max} - E_{1/2} \quad (7)$$

and upon further manipulation produces the following expression for  $\alpha$ :

$$\alpha = \frac{1}{1 + \exp\left(\frac{nF\Delta E}{RT}\right)} \quad (8)$$

Using this expression for the transfer coefficient, the data for the half-wave potential provided by CLB, and the phase angle versus potential data in the results section, values of the transfer coefficient for the two faradaic reactions ( $\text{Ti}^{3+}/\text{Ti}^{2+}$  at  $-0.8$  V and  $\text{Ti}^{2+}/\text{Ti}^0$  at  $-1.2$  V) can be determined. The temperature for all of the calculations is  $T = 1003\text{K}$ .

For  $E_{1/2} = -0.8$  V:

$$n = 1 \quad \Delta E = + 0.061 \text{ V and yields}$$

$$\alpha = \frac{1}{1 + 2.03} = 0.33 \quad (9)$$

For  $E_{1/2} = -1.2$  V:

$n = 2$        $\Delta E = -0.04$  V and yields

$$\alpha = \frac{1}{1 + 0.40} = 0.72 \quad (10)$$

These results give insight to the ease of transition between the various species. The natures of the activation energy barriers for the three values of the transfer coefficient ( $\alpha > 0.5$ ,  $\alpha < 0.5$ ,  $\alpha = 0.5$ ) are shown schematically in Figure 17. In the absence of other information, a faradaic reaction is usually assumed to have a transfer coefficient of  $\alpha = 0.5$ , which means that the energy barrier is of exactly the same nature for the forward and reverse reactions. However, in the  $\text{Ti}^{3+}/\text{Ti}^{2+}$  reaction, carried out on a glassy carbon electrode, the transfer coefficient is less than 0.5, with a value of 0.33 as calculated above. This indicates that the energy barrier for the forward reaction is less steep than the energy barrier for the reverse reaction. However, for the  $\text{Ti}^{2+}/\text{Ti}^0$

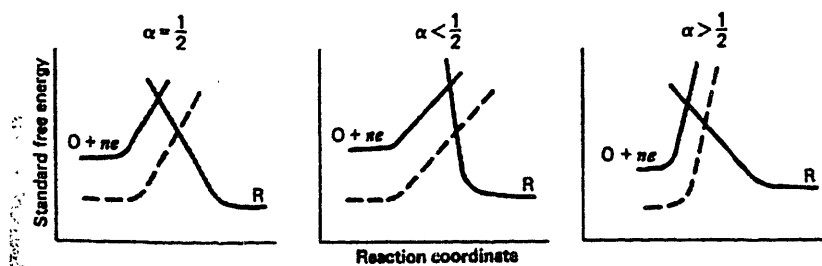


**Figure 17: Schematic of the variation of the symmetry of the energy barrier for different values of the transfer coefficient. From Bard & Faulkner, 1980, p.97.**

reaction the transfer coefficient is greater than 0.5 ( $\alpha = 0.72$ ) and hence the energy barrier for the forward reaction is steeper than the energy barrier for the reaction from solid back to the divalent species in solution. The transfer coefficient does not indicate the relative stability of the two species in a redox couple; relative stability is set by difference in the minima of the free energy curve, the shape of which is altered based on the applied potential, all other variables being equal. The transfer coefficient identifies the slope of the free energy curve in the vicinity of the activated state. A species that must follow a steep free energy slope approaching the activated state is more sensitive to changes in potential. Small changes in potential lead to drastic changes in the amount of energy it takes to reach the activated state. For the chlorotitanates, the divalent species are the ones that have a severe sensitivity to changes of potential. Hence the reactions which consume the divalent species, either:



or



have a steep energy barrier and are extremely sensitive to changes of potential as compared to the reverse reactions. Furthermore, this indicates that the overvoltages for the two reactions above, carried out on a glassy carbon electrode, should be relatively low, whereas for the reverse reactions they should be relatively high.

However, this explanation begs the question of what the transfer coefficient means. Electrochemical reactions have the unique quality that their reactions can have asymmetric energy barriers. This means that for  $\alpha \neq 0.5$ , equal magnitude anodic and cathodic voltage excursions will cause unequal current responses. The current-potential characteristic is shown schematically in Figure 18 for three values of  $\alpha$ . Notice the asymmetry of the  $\alpha = 0.25$  and  $\alpha = 0.75$  curves. Changes in the activation barrier for the

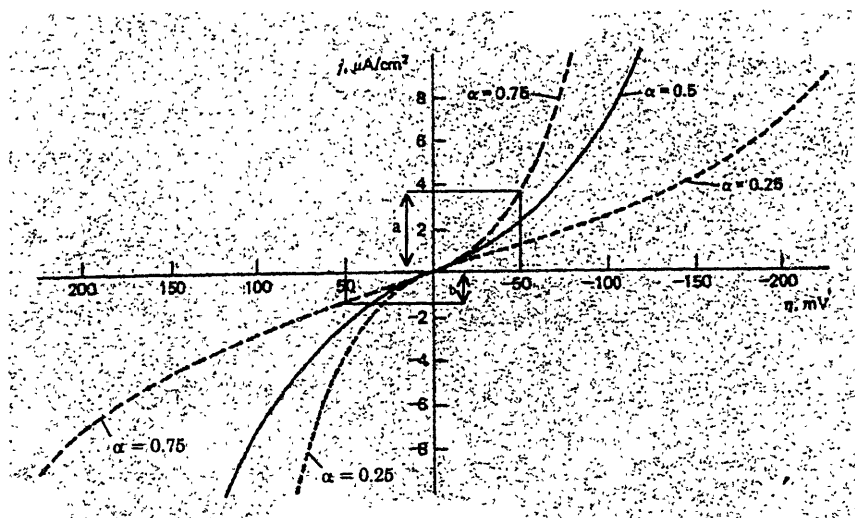


**Figure 18: Effect of the transfer coefficient on the symmetry of the current-overpotential curves. Notice that  $-50$  mV produces “a” current response which is almost 3 times “b” which is the current response for  $+50$  mV. From Bard & Faulkner, p.104.**

forward and reverse reactions become dependent on potential. This potential dependence arises because the electrochemical reaction is driven not only by temperature but also by changes in the population of electrons on the electrode. These electrons must be able to leave (or enter) the electrode, and the case of  $\alpha \neq 0.5$  describes a situation in which the activation changes disproportionately for the donation versus the accepting reactions. In order for an electrode to be able to donate or accept electrons, the energy states of the electrode and the ions need to match. Hence the work function and density of states distribution in the metal and redox species determine the value of the transfer coefficient.

The second piece of kinetic information which can be elucidated is the standard rate constant,  $k^0$ . The standard rate constant identifies the “idle speed” at which the reaction proceeds on the substrate used as the working electrode. A reaction with fast kinetics has a high standard rate constant with values on the order of  $10^{-2}$  cm/sec. A reaction with slow kinetics has a much smaller  $k^0$  value, typically three or more orders of magnitude lower at about  $10^{-5}$  cm/sec.

The value of the standard rate constant is accessible via the variation of the phase angle with the frequency of the ac potential ripple at the half wave potential. The expression for this relationship is:

$$[\cot\phi]_{E_{1/2}} = 1 + \frac{\omega^{1/2}}{k^0} \sqrt{\frac{D_O^\beta D_R^\alpha}{2}} \quad (13)$$



where  $\alpha$  and  $\beta$  are the transfer coefficients as defined previously,  $\omega$  is the angular frequency of the ac ripple, and  $D_O$  and  $D_R$  are the diffusion coefficients for the oxidized and reduced species, respectively. If these data fall on a line with a y-intercept value of 1 then the system is well behaved and the slope of the line reveals the standard rate constant based on the relation:

$$k^0 = \frac{1}{m} \sqrt{\frac{D_O^\beta D_R^\alpha}{2}} \quad (14)$$

where  $m$  is the slope of the line in a plot of  $\cot\phi$  vs  $\omega^{1/2}$ .

Based on the data reported in the previous section, there are two characteristic potentials at which faradaic processes have been identified. The first reaction is the  $Ti^{3+}/Ti^{2+}$  couple which has a half-wave potential of  $-0.8$  V. Measuring the values of  $\cot\phi$  at this potential for two different values of frequency gives the relation shown in Figure 19. The statistics for linear

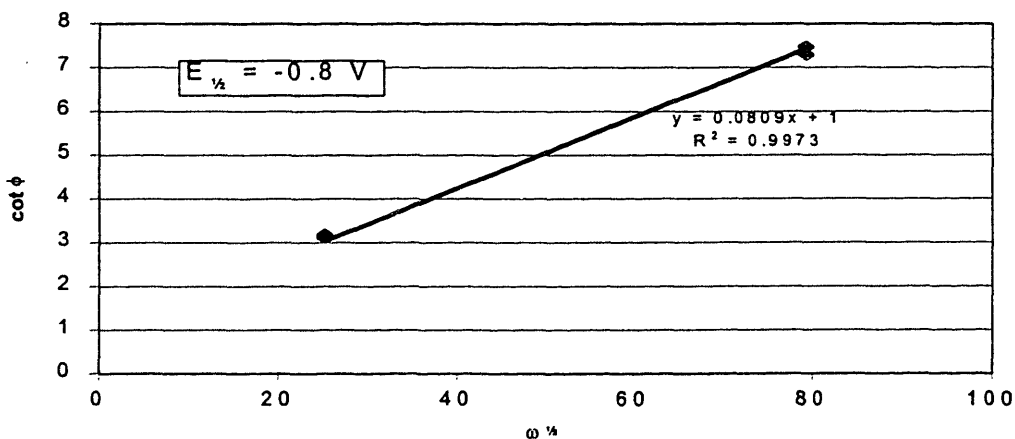


Figure 19:  $\cot\phi$  vs  $\omega^{1/2}$  for  $Ti^{3+}/Ti^{2+}$ .

regression fit are included in the figure and show a slope of 0.0809. Using this value for  $m$  and using  $D_O = D_R = 3.76 \times 10^{-5} \text{ cm}^2/\text{sec}$ , the calculated value for  $k^\circ$  is  $5.4 \times 10^{-2} \text{ cm}/\text{sec}$ .<sup>1,2</sup> This is a relatively large value for the standard rate constant and is an indication that this reaction is fast.

The half-wave potential for the  $\text{Ti}^{2+}/\text{Ti}^0$  couple is  $-1.2 \text{ V}$ . The above analysis produces the data in Figure 20. The value of the slope is 0.6976 and the resulting value for  $k^\circ$  is calculated to be  $6.2 \times 10^{-3} \text{ cm}/\text{sec}$ , which is about an order of magnitude lower than the value for  $\text{Ti}^{3+}/\text{Ti}^{2+}$ .

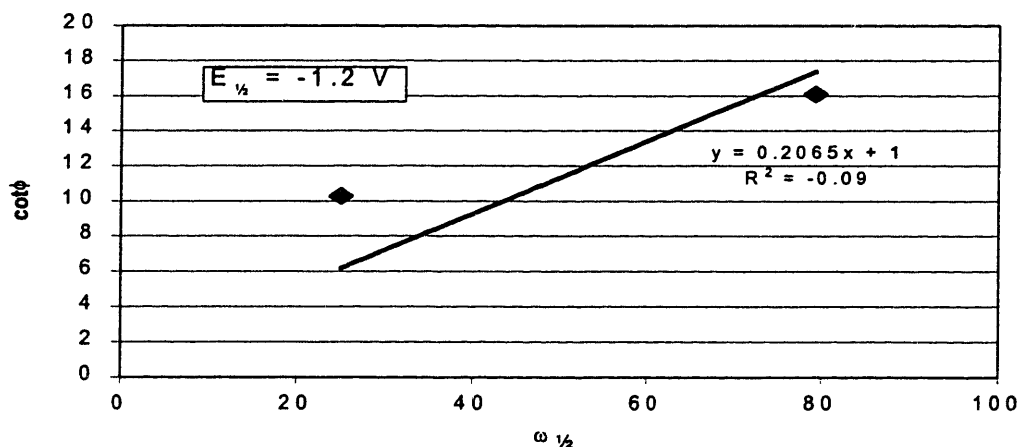


Figure 20:  $\cot \phi$  vs  $\omega^{1/2}$  for  $\text{Ti}^{2+}/\text{Ti}^0$ .

<sup>1</sup> This value is based on the calculation of the diffusion coefficient for the trivalent and tetravalent titanium species in NaCl-KCl at 973K based on the data reported in the Journal of Physical and Chemical Reference Data, Vol 11, No. 3, p.596.  $D_{\text{Ti}^{3+}} = 3.76 \times 10^{-5} \text{ cm}^2/\text{sec}$ ,  $D_{\text{Ti}^{4+}} = 1.91 \times 10^{-5} \text{ cm}^2/\text{sec}$ .

<sup>2</sup> For the calculation of  $k^\circ$ ,  $D_{\text{Ti}^{2+}}$  is assumed to be close enough in value to  $D_{\text{Ti}^{3+}}$  that the same value can be used for both. This strength of this assumption has been discussed elsewhere (Ferry, 1987) where its appropriateness was supported experimentally.

## 2.7 SUMMARY OF SCIENTIFIC FINDINGS

The electroanalytical experiments have:

1. Confirmed the characteristic half-wave potentials ( $E_{1/2}$ ) of previous studies with ac techniques. The potentials (expressed with respect to a Ag/Ag<sup>+</sup> reference electrode) are:

$Ti^{4+}_{complex}/Ti^{3+}$	+0.25 V
$Ti^{4+}_{gas}/Ti^{3+}$	-0.20 V
$Ti^{3+}/Ti^{2+}$	-0.80 V
$Ti^{2+}/Ti^0$	-1.20 V

2. Explained the features of the ac voltammograms for the through the assignment of faradaic reactions.
3. Determined the values of the transfer coefficient,  $\alpha$ , for the  $Ti^{3+}/Ti^{2+}$  and  $Ti^{2+}/Ti^0$  couples on glassy carbon.

$Ti^{3+}/Ti^{2+}$	0.33
$Ti^{2+}/Ti^0$	0.72

4. Determined the values of the standard rate constants,  $k^0$ , for the  $Ti^{3+}/Ti^{2+}$  and  $Ti^{2+}/Ti^0$  couples on glassy carbon at 730°C.

$Ti^{3+}/Ti^{2+}$	$5.4 \times 10^{-2}$ cm/sec
$Ti^{2+}/Ti^0$	$6.2 \times 10^{-3}$ cm/sec

5. Established that the slow step in the deposition of Ti metal from a chlorotitanate melt is reduction from  $Ti^{2+}$  to metal.

## 3.0 Spectroscopy

### 3.1 SUMMARY

Spectroscopic investigation has characterized the structure of the chlorotitanate complexes in the bulk melt. Raman spectroscopy and absorption spectroscopy have established that:

- a temperature sensitive equilibrium exists between  $\text{TiCl}_6^{3-}$  and  $\text{TiCl}_4^-$  in the eutectic; and,
- the concentration of  $\text{Ti}^{3+}$ , as well as additions of  $\text{Ti}^{2+}$ , can be accurately sensed via fiber optic absorption spectroscopy; and,
- Raman spectroscopy is ill suited for investigating complexation in the molten chlorotitanates.

### 3.2 BACKGROUND

While electrochemical refining of titanium is an interfacial process, bulk chemistry has a strong influence on efficiency, including faradaic yield and metal purity. In order to investigate the bulk chemistry of the chlorotitanates, the use of non-invasive spectral probes has been explored. The basic mode of operation common to all these techniques is to irradiate the sample in order to promote electronic and/or vibrational transitions. These transitions generate a secondary emission which is collected. The wavelength of the light stimulus is varied and the corresponding change in response is recorded in order to provide insight into the structure/composition of the melt. This is shown schematically in Figure 21.

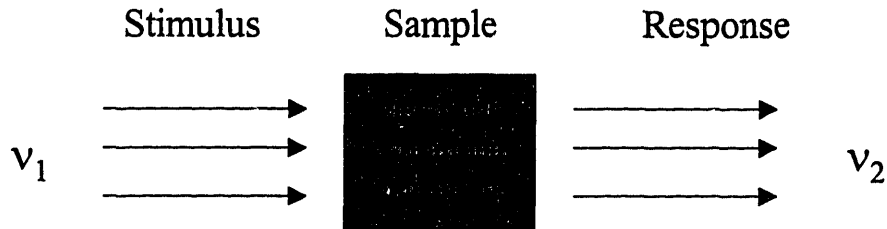


**Figure 21: Schematic representation of spectroscopic methods.**

In Raman spectroscopy the stimulus is monochromatic visible light (typically the 488 nm or 514 nm laser line for  $\text{Ar}^+$ ). The response signal is analyzed for the spectrum of wavelengths it contains. The laser excitation probes the covalent bonds of the various chloro-complexes in the melt. The bond energy is related to the shift of wavelength between stimulus and response. Furthermore, the number and phase sensitivity of peaks indicates the coordination of the active species. Raman spectroscopy is an established field and the selection values for the number of peaks and their polarization sensitivity has been catalogued for numerous configurations of polyatomic covalent species. (Ferraro & Nakamoto, 1994)

The electronic transitions within a sample are investigated by illuminating the sample with polychromatic light and measuring the amount of transmitted light that reaches the detector at chosen wavelengths. The intensity of the electronic transitions in dilute solutions follows Beer's law.

This law states that for a wavelength,  $\lambda$ , the relationship between absorbance,  $A$ , and concentration,  $c$  (mol/L) is:

$$A_{\lambda} = \epsilon_{\lambda} c l \quad (15)$$

with  $\epsilon$  (L/mol·cm) as the molar absorptivity and  $l$  as the optical path length (cm). The energies at which absorption peaks occur correlate to the allowed electronic transitions in titanium with various ligand coordinations. Selection rules are described in various texts on the subject of spectroscopy. An understandable and complete treatment of the subject is provided in the first chapter of *Introductory Raman Spectroscopy* (Ferraro & Nakamoto, 1994).

### 3.3 EARLIER WORK

#### *Raman investigations of titanium ions in low temperature melts and solid state*

As early as 1962, spectroscopic studies of titanium complexes were being performed. (Gruen & McBeth, 1963) There is a long list of the studies of titanium complexes, (Adams, 1968; Crouch, 1969; van Bronswyk, 1969) but they suffer from two weaknesses as relates to the current study. First, with the exceptions noted below, these studies deal exclusively with tetravalent titanium species. Second, the spectra have been recorded in room temperature molten salt systems or in the solid state. The main finding of the studies was that tetravalent titanium forms chloro-complexes, mostly of six-coordination. The wavenumber shifts ( $\Delta\nu$ ) characteristic of the various Raman active vibrational modes were also reported for the complexes studied.

As mentioned above, there have been a few studies of systems other than the  $Ti^{4+}$  systems as well as little high temperature Raman work.  $Ti^{3+}$  has been studied in the solid state (Fraser, 1977; Chassaing, 1980a) as well as in high temperature molten salt systems.(Chassaing, 1980b; Chassaing, 1981) The later study proposed an equilibrium between  $TiCl_6^{3-}$  and  $TiCl_4^-$  based on the cationic radius of the alkali species and non-obvious peak assignments. Also, evidence for the  $Ti_2Cl_9^{3-}$  complex was presented. The solid state Raman work (Fraser, 1977) is shown in Figure 22 for  $\beta-TiCl_3$  (there are three isomorphs of  $TiCl_3$ :  $\alpha$ ,  $\beta$  and  $\gamma$ ).  $\alpha-TiCl_3$  and  $\beta$  are expected to have a similar Raman response as they are both based on a layered structure as opposed to the linear fibrous structure of the  $\gamma$ -form. Two major peaks are detected at  $\Delta\nu = 224\text{ cm}^{-1}$  and  $366\text{ cm}^{-1}$ , with the lower energy band having the higher intensity.

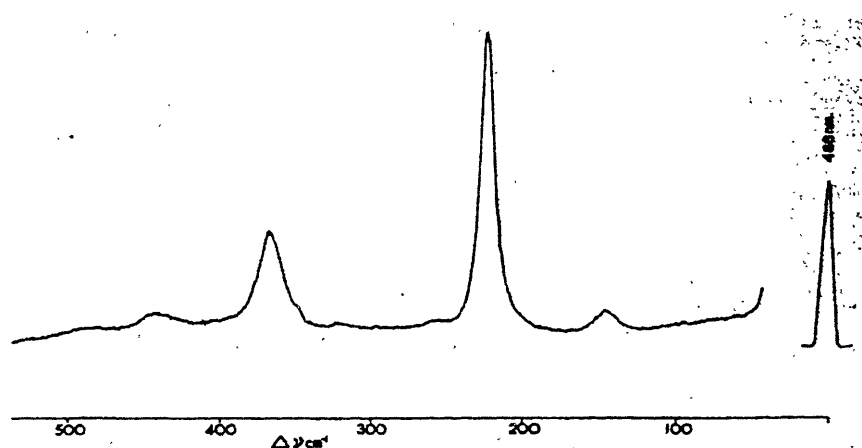


**Figure 22: Stokes Raman spectrum of  $\beta-TiCl_3$  at room temperature. From Fraser, et al, 1977.**

### *UV/Visible/IR studies of titanium complexation*

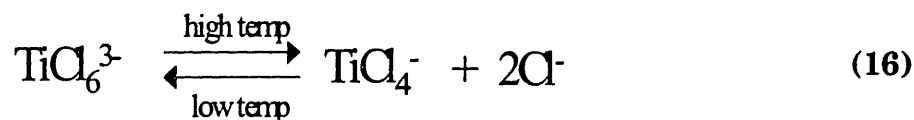
There have also been infra-red and UV/visible investigations of the tetravalent titanium chloro-complexes. (Wendling, 1967; Clark, 1968; Creighton, 1968) These studies confirm the coordination results from the Raman studies as well as providing information about those vibrational modes that are uniquely IR active.

Of particular note is the work of Sørliie & Øye. The initial work involved an investigation of the stability of the titanium chlorides in gaseous aluminum chloride via absorption spectroscopy. (Sørliie, 1978) After identifying the possibility for developing a chemical vapor deposition process for metallic titanium, the behavior of titanium chlorides in fused salt solvents was studied. The absorption behavior of the titanium chlorides in fused chloroaluminates was examined extensively in  $\text{AlCl}_3$ ,  $\text{AlCl}_3\text{-KCl}$  as well as  $\text{LiCl-KCl}$ . (Sørliie, 1981)  $\text{Ti}^{3+}$  has a six-coordination in pure  $\text{AlCl}_{3(l)}$  and high aluminum chloride concentrations of  $\text{AlCl}_3\text{-KCl}$  melts. Low aluminum chloride containing  $\text{AlCl}_3\text{-KCl}$  melts show six/four-coordination equilibria.  $\text{Ti}^{2+}$  is also six-coordinated for high  $\text{AlCl}_3$  concentrations, with a propensity to become unstable via disproportionation at lower  $\text{AlCl}_3$  concentrations.

Based on the limited experimentation using the  $\text{LiCl-KCl}$  system (Figure 23 shows  $\text{Ti}^{3+}$  spectra and Figure 24 shows  $\text{Ti}^{2+}$  spectra), Sørliie & Øye were able to provide the analysis summarized below. Trivalent titanium ( $\text{Ti}^{3+}$ )



has the  $d^1$  electronic configuration. This electronic structure has three degenerate ground states and two degenerate excited states. Sørli & Øye detected an absorption band at  $13,500\text{cm}^{-1}$  and attributed it to the  $d \rightarrow d$  transition  ${}^2T_{2g} \rightarrow {}^2E_g$  in the octahedrally symmetric complex  $\text{TiCl}_6^{3-}$ . This was a double band with a shoulder at  $10,700\text{cm}^{-1}$  which broadens (lowering of octahedral symmetry) and red shifts (vibrational effects) as temperature increases. A second band was identified at  $6,400\text{cm}^{-1}$  and was attributed to the  ${}^2E \rightarrow {}^2T_2$  transition in four-coordinate  $\text{TiCl}_4^-$ . Based on this the following equilibrium is proposed for  $\text{Ti}^{3+}$ :



Divalent titanium ion ( $\text{Ti}^{2+}$ ) has the  $d^2$  electronic configuration which has three spin-allowed electronic transitions; each of these is seen in the

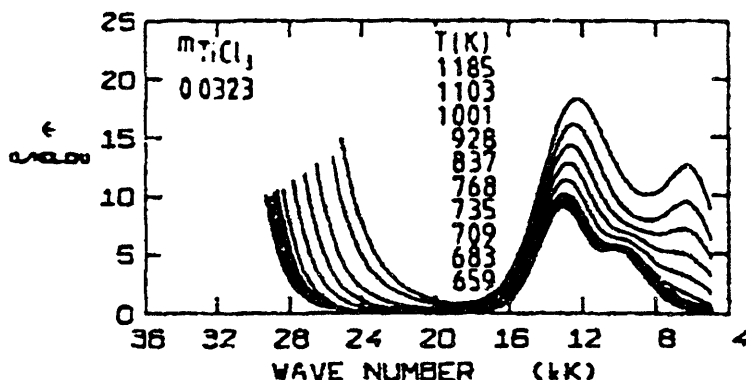


Figure 23: Absorption spectra for 32.3 milli-molal  $\text{TiCl}_3$  in  $\text{LiCl-KCl}$  at various temperatures. From Sørli and Øye, 1981

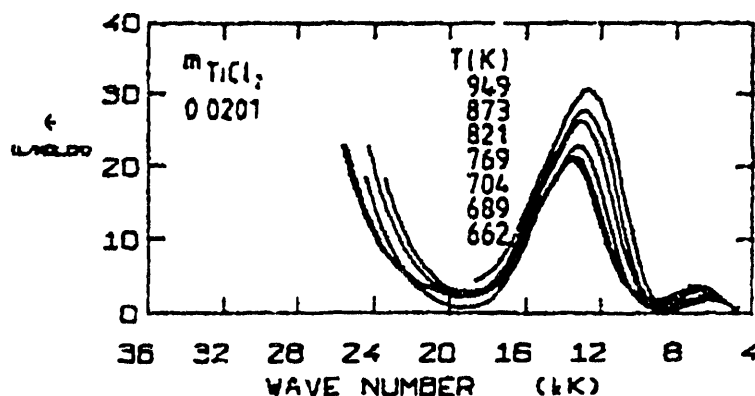


Figure 24: Absorption spectra for 20.1 milli-molal  $\text{TiCl}_2$  in LiCl-KCl eutectic at various temperatures. Sørli and Øye, 1981

absorption spectrum; none of them is temperature sensitive. The  $13,550\text{cm}^{-1}$  band is assigned to the  ${}^3\text{T}_{1g}(\text{F}) \Rightarrow {}^3\text{T}_{1g}(\text{P})$  and the  $6,950\text{cm}^{-1}$  band is due to  ${}^3\text{T}_{1g}(\text{F}) \Rightarrow {}^3\text{T}_{2g}(\text{F})$  and the shoulder at  $15,000\text{cm}^{-1}$  to the weak transition  ${}^3\text{T}_{1g}(\text{F}) \Rightarrow {}^2\text{A}_{2g}(\text{F})$ . The analysis of the energy levels for the transitions leads to the conclusion that  $\text{Ti}^{2+}$  is six-coordinated in this system at all temperatures studied.

#### *Fiber optic investigation of the Raman response in high temperature corrosive melts*

The use of fiber optic probes to investigate the Raman response has been employed for more than fifteen years. (Schwab, 1984) Recently, that technique has been applied to investigating high temperature molten salt systems. (Dai, 1992)

In order to use spectroscopic analysis toward quantitative goals, it is necessary to have a calibration curve for the system being investigated. This curve gives the relationship between species concentration and measured

intensity for a characteristic peak of the complex studied. Another important characteristic of the calibration curve is that it becomes non-linear as multiple species become present in the same melt. Band resolution techniques (such as factor analysis and pseudo-isosbestic points) have been used to eliminate the non-linear nature of the calibration curve as well as to identify the relative amounts of each species present. These techniques have found application in both vibrational as well as absorption spectroscopy analysis. (Dai, 1995; Bulmer, 1973)

### **3.4 EXPERIMENTAL/APPARATUS/TECHNIQUES**

The spectroscopic investigations were conducted at Oak Ridge National Laboratory. The Raman experiments were carried out using two separate experimental set-ups, one for melts and one for solids. The molten salt results were recorded using the fiber optic arrangement shown schematically in Figure 22 and described in Dai, et al. (1992) The source was the 514 nm line from an Ar<sup>+</sup> laser (Coherent) and the backscatter geometry was employed. The solid Raman results were obtained in experiments at the High Temperature Materials Laboratory at ORNL. The fiber optic system was employed with the same laser source and an Instruments SA Dilor XY800 spectrographic set-up. The well characterized Raman spectrum for carbon tetrachloride at room temperature was used as the calibration standard.

All of the absorption spectroscopy was performed with the same instrument. The Cary-14 spectrophotometer converted by On-Line Instrument Systems (OLIS) for data acquisition by an IBM-AT personal computer was used for all absorption spectroscopy experiments. A Watlow resistance furnace was placed in the light path between the source and detector on the spectrophotometer. The system was also fitted with an interface system that allowed for experiments employing fiber optic techniques (as described in Dai, et al, 1994) as shown in Figure 25. In the present study

fiber optic techniques were employed only as *ex situ* analysis tools to assess their utility with chlorotitanate melts.

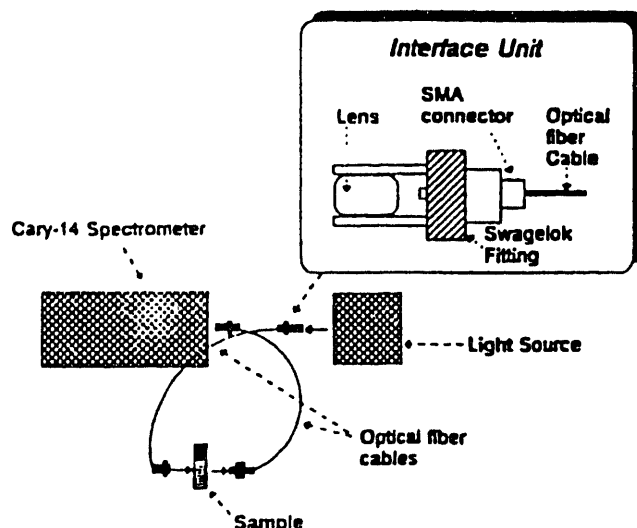


**Figure 25: Fiber optic interface system and the standard spectrographic set-up for absorption experiments.**

The salts used for the spectroscopic studies were prepared as described in Chapter Two. All samples were handled in a helium filled glove box where they were weighed, inserted into fused quartz sample holders, and sealed with a threaded glass connector cap. These samples were then placed in the resistance furnace and entire hot zone was aligned so as to assure maximum signal and proper incidence with the light source. The sample holder is drawn schematically in Figure 26 and the entire arrangement is shown in Figure 25. The furnace was placed into the system between the light source and the spectrometer where the optical fibers are located in Figure 25.

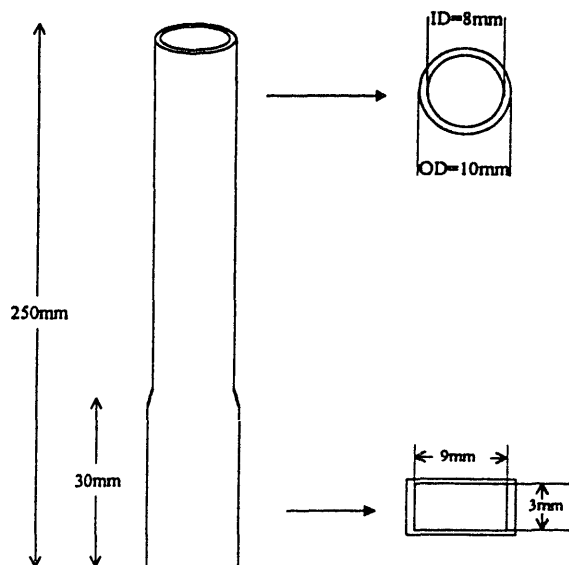


**Figure 26: Fused quartz spectroscopic cell**

A baseline spectrum was recorded with the furnace at temperature and a sample holder in the beam path (either empty or containing the supporting electrolyte).

### 3.5 RESULTS

#### *Raman Spectroscopy*

To study how speciation varies with composition Raman spectra were recorded for various melts. Solid state samples were included in the study. The Ar<sup>+</sup> 514 nm laser line (set to 100 mW laser power) was employed to study the Raman response of K<sub>2</sub>TiCl<sub>6</sub> (68 wt% in KCl) at room temperature. The shift in frequency of the back-scattered light was recorded and converted to wavenumber (cm<sup>-1</sup>). Figure 25 shows the intensity of the reflected light recorded for each increment in energy (wavenumber) away from the excitation line. The Stokes lines (excitations with negative wavenumber shifts from the excitation source) are presented here as their signal is more intense than the anti-Stokes lines (positive wavenumber shift). As seen in Figure 27, there are two strong peaks at 188 cm<sup>-1</sup> and 334 cm<sup>-1</sup>, and, as shown in Figure 28, a shoulder at ~430 cm<sup>-1</sup> and a weak peak at 660 cm<sup>-1</sup>. Because this is a solid

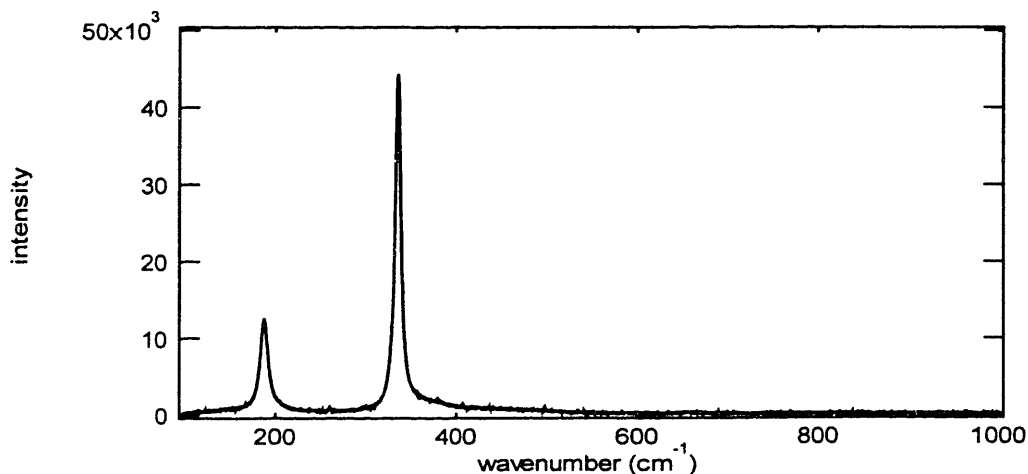
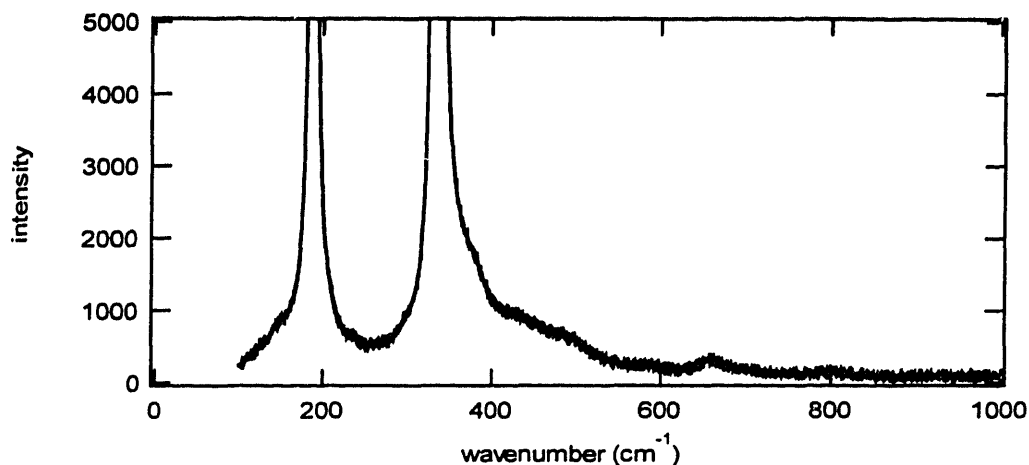


Figure 27: Raman spectrum of K<sub>2</sub>TiCl<sub>6</sub> in KCl at 25°C (solid).



**Figure 28: Expanded view of above. Notice the two high energy peaks.**

sample, the polarization sensitivity of these peaks cannot be investigated.

Figure 29 shows the spectrum for  $\text{TiCl}_3$ . The  $\text{TiCl}_3$  was analyzed in its pure form at room temperature using the  $\text{Ar}^+$  514 nm line with the laser power set to 100 mW. This sample produces only two discernible peaks. The first peak at  $223 \text{ cm}^{-1}$  is the stronger peak, with a less intense peak at  $365 \text{ cm}^{-1}$ . There is a broad shoulder at higher energies which is attributed to the glass in the sample holder and the optics.



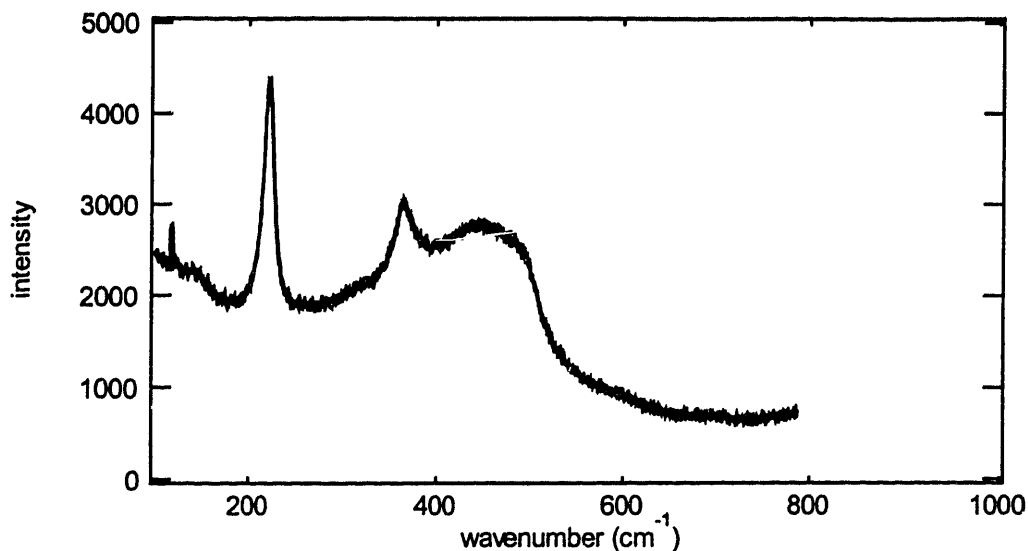


**Figure 29:  $\text{TiCl}_3$  Solid Raman spectrum**

The high temperature Raman experiments produced largely unsatisfying results. A typical spectrum for  $\text{K}_2\text{TiCl}_6$  (287 mM in CsCl-NaCl-KCl eutectic) at high temperature is shown in Figure 30. Both the Stokes and anti-Stokes lines are included for completeness. The overall intensity of the

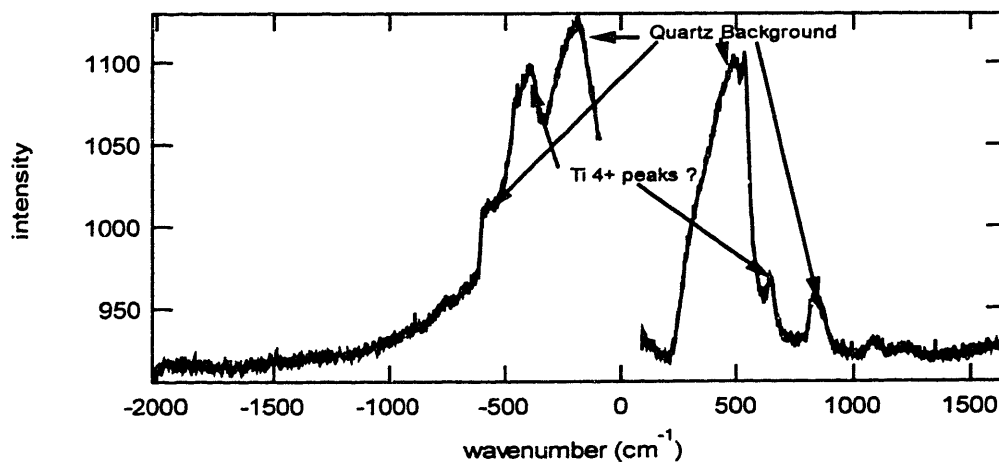


**Figure 30:  $\text{K}_2\text{TiCl}_6$  287 mM in CsCl-NaCl-KCl at 660°C.**

signal is much lower in the high temperature case, but the peak at ( $\sim 650\text{ cm}^{-1}$ ) appears to be evident but shifted to lower energies than observed in the solid state experiments. The fused quartz vessel used to contain the melt is Raman active as well as the optical fiber. This gives rise to a background signal containing a few peaks which are especially prominent based on the extremely low intensity of the Raman signal due to the low concentration of the Raman active  $\text{TiCl}_6^{2-}$  species. Due to the deeply colored nature of the melts, addition of more  $\text{K}_2\text{TiCl}_6$  did not increase the intensity of the peaks. Instead, more concentrated melts were darker and the already weak Raman signal was absorbed by the melt.

### *Absorption Spectroscopy*

UV/Visible/Near-IR absorption spectroscopy probes electronic transitions within a melt. This study focused on the high temperature behavior of chlorotitanate melts. The lack of valence shell electrons leaves the  $\text{Ti}^{4+}$  spectra rather uninteresting since only high-energy UV transitions (charge transfer from the metal to ligand) are possible. The instability of  $\text{TiCl}_2$  in these melts led to rapid disproportionation when added as the only source of titanium ions. Consequently, the spectra for melts containing  $\text{TiCl}_3$  are presented as well as those with a mix of  $\text{TiCl}_3$  and  $\text{TiCl}_2$  (added in sparing amounts).

A melt was prepared with 330 mM  $\text{Ti}^{3+}$  dissolved in CsCl-NaCl-KCl. The absorption spectrum was recorded over a range of wavelengths from 2200 nm (near-IR) to 350 nm (UV). The absorption values are plotted versus wavenumber and the spectra for temperatures from 582°C to 730°C are shown in Figure 31. An absorption value of 5 on this scale corresponds to complete absorption by the sample. All of the spectra show a charge transfer band in the high energy UV range ( $\sim 25,000 \text{ cm}^{-1}$  and higher). The low temperature spectrum has three features. There is a high energy peak at  $12,700 \text{ cm}^{-1}$  and low energy peak at  $6,000 \text{ cm}^{-1}$ . There is also a shoulder at  $9,100 \text{ cm}^{-1}$ . At increased temperature, the intensity of the low energy peak increases while the shoulder disappears. The high energy peak shows little sensitivity to temperature over the  $150^\circ\text{C}$  range investigated.

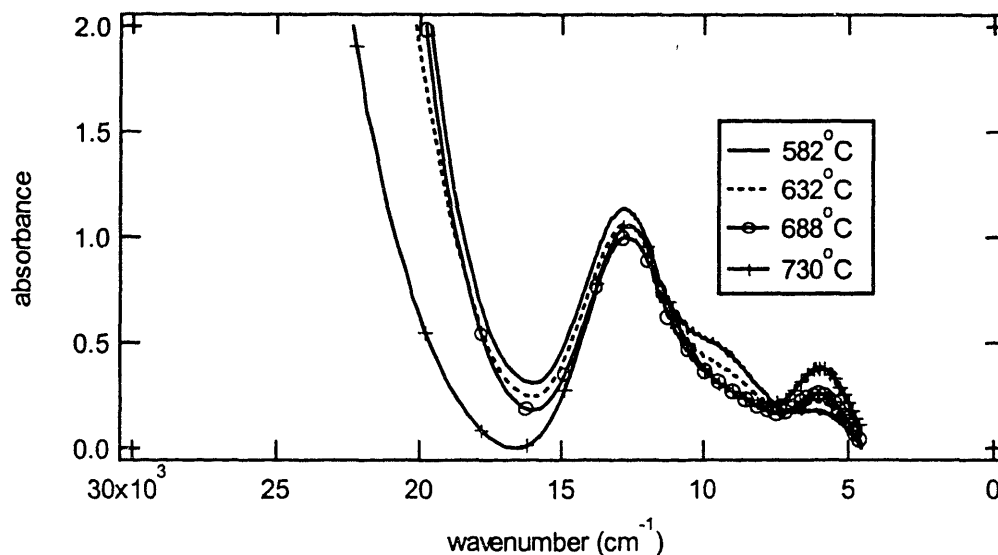


**Figure 31: Absorption spectrum for  $\text{Ti}^{3+}$ , 330 mM in CsCl-NaCl-KCl, temperature as indicated.**

Isothermal variation of the absorption spectrum with  $\text{Ti}^{3+}$  concentration is shown in Figure 32. The high energy charge transfer band is still apparent, and at this temperature ( $688^\circ\text{C}$ ) the predominant features are the high energy and low energy peaks as identified above. The intensity of the shoulder is not pronounced but it is still apparent. The increase in concentration from 122 mM to 404 mM produced spectra with increased absorption peak heights corresponding to the change in concentration as expected by Beer's law. With the same spectrometer and source, but employing a fiber optic light path to the melt, a series of absorption spectra was recorded for various concentrations of  $\text{Ti}^{3+}$ . Figure 33 shows how the variation in concentration affected the high-energy peak when the fiber optic assembly was employed. The system seems to obey the Beer relation over this range of concentration.

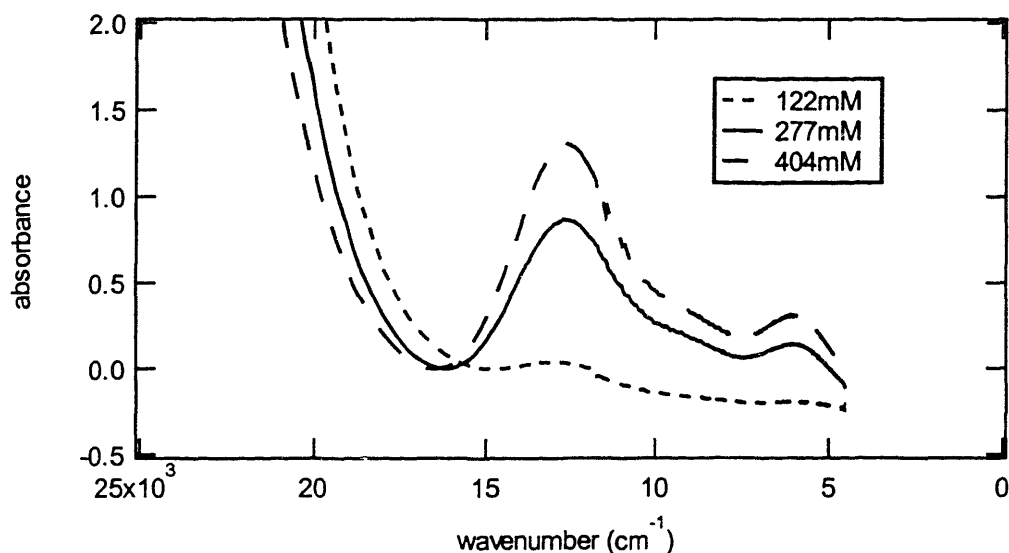


**Figure 32: Absorption spectrum of  $\text{TiCl}_3$  at varying concentrations. Temperature was constant at  $688^\circ\text{C}$ .**

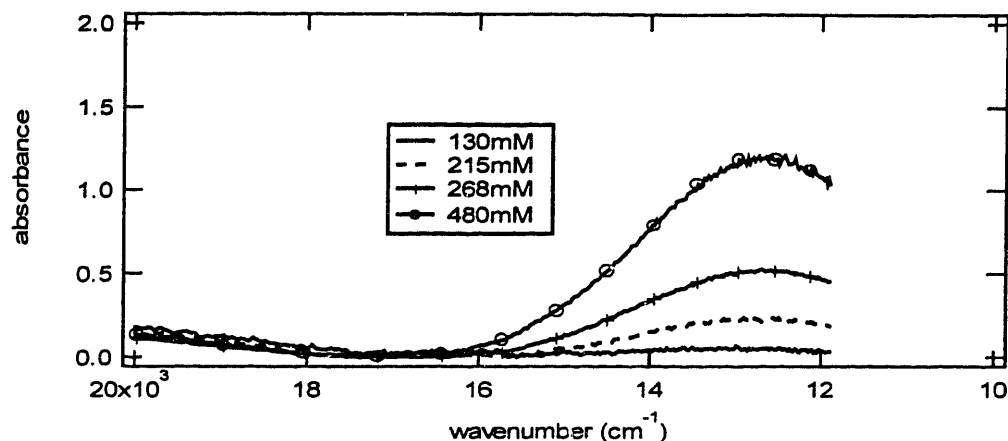


**Figure 33: Absorption spectrum for  $\text{TiCl}_3$  at various concentrations. Recorded using a fiber optic collection system  $688^\circ\text{C}$ .**

Melts consisting of  $\text{TiCl}_2$  dissolved in the eutectic were unstable and produced a thin metal coating on the optical cell which is attributed to the disproportionation of the  $\text{Ti}^{2+}$  into  $\text{Ti}^{3+}$  and solid titanium. This metallization of the optical cell impaired the ability to record absorption spectra for these melts. However, it was possible to record absorption spectra were by adding  $\text{TiCl}_2$  in small amounts to a  $\text{TiCl}_3$ -containing melt. A 404 mM  $\text{TiCl}_3$  melt was prepared and its absorption spectrum was recorded.  $\text{TiCl}_2$  was added in small amounts and for each addition the new absorption spectrum was recorded. The ratio of  $\text{TiCl}_3$  to  $\text{TiCl}_2$  added ranged from 50:1 to 6:1. The spectra recorded at  $688^\circ\text{C}$  for the various concentrations are shown in Figure 34. The features remain at the same energy with a noticeable increase in magnitude as  $\text{Ti}^{2+}$  is added.

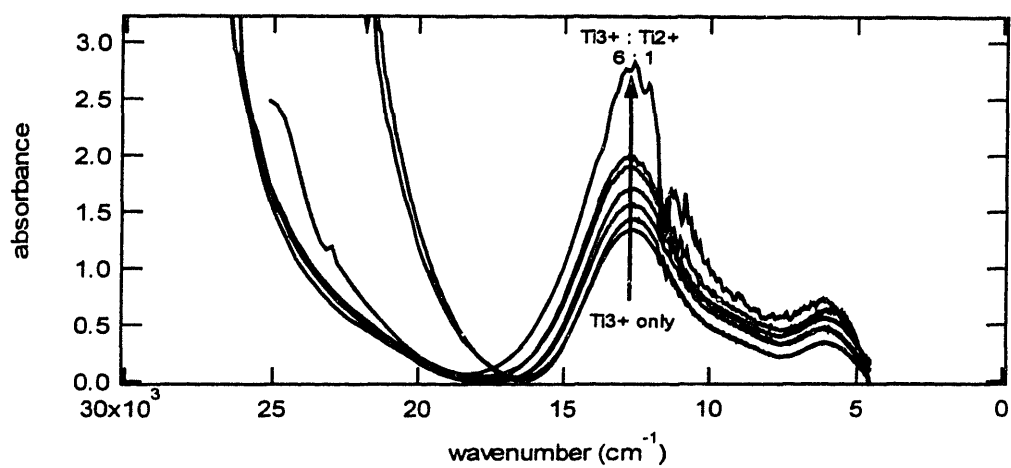


**Figure 34: Absorption spectrum of  $\text{TiCl}_2$ , added to  $\text{TiCl}_3$ , in the eutectic electrolyte at  $688^\circ\text{C}$ . Ratios vary from  $\text{Ti}^{3+}$  only to 6:1  $\text{TiCl}_3$  to  $\text{TiCl}_2$  (intermediate ratios were 50:1, 30:1, 20:1, 8:1, 7:1).**

### 3.6 DISCUSSION

There was much optimism for the application of Raman spectroscopy based on previous experience in this laboratory working with molten salts containing transition-metal ions. (Kipouros, 1985) However, due to the opacity of the chlorotitanate melts, the Raman signal was detectable because it was either absorbed by the melt (at high concentrations) or too weak (at low concentrations). The results for solid  $\text{TiCl}_3$  measured in the study are in agreement with previously reported values.

Absorption spectroscopy was more successful. Prior work by Sørli and Øye identified three absorption peaks for  $\text{TiCl}_3$  in  $\text{LiCl-KCl}$ . The absorption bands for the present study are red shifted by about  $700\text{ cm}^{-1}$  to  $900\text{ cm}^{-1}$ . Sørli and Øye also recorded the temperature dependence of the two low energy peaks in their study. There is nothing in the results of the present study to dispute the electronic transitions assigned by Sørli and Øye to the various bands. Hence, the  $12,700\text{ cm}^{-1}$  band in the present work is due to a  $d \Rightarrow d$  transition  ${}^2T_{2g} \Rightarrow {}^2E_g$  in a six-coordinate species such as  $\text{TiCl}_6^{3-}$ . The  $6,000\text{ cm}^{-1}$  band is attributed to a  ${}^2E \Rightarrow {}^2T_2$  transition four-coordinate  $\text{Ti}^{3+}$ .

Also, the same disproportionation reaction was observed when  $\text{Ti}^{2+}$  was the only titanium species present. The metallization reaction at the optical cell wall was slower than experienced in the present study, so there was sufficient

time to record spectra before the sample was obscured. This seems to be related to their solvent system and the process by which  $\text{TiCl}_2$  was produced.

The present study not only verified the results of Sørli and Øye using a different solvent system, but also provided the basis for quantitative analysis of melt composition. Figure 35 shows the variation of peak (or maximum) absorbance at  $12,700\text{ cm}^{-1}$  with concentration. The data fit well on a line with

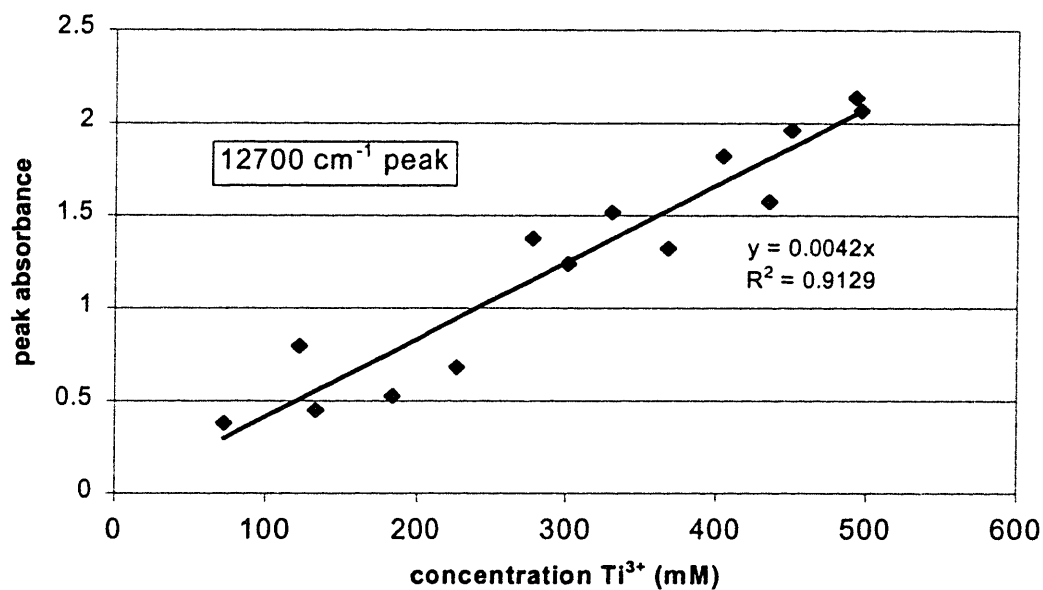


**Figure 35: Concentration calibration curve for absorption peak at  $12,700\text{cm}^{-1}$ . Temperature is  $688^\circ\text{C}$ .**



the origin as its intercept. The value of the slope,  $4.2 \times 10^{-3} \text{ (mM}^{-1}\text{)}$ , is steep enough that a 2.5 mM change in concentration corresponds to a change of 0.01 absorbance units which is well within the detection limits of the instrument and the technique.

The calibration curve for the low energy peak at  $6000 \text{ cm}^{-1}$  is presented in Figure 36 and is sensitive to concentration changes. The slope of  $1.3 \times 10^{-3} \text{ (mM}^{-1}\text{)}$ , implies that a fluctuation of 10 mM in concentration will produce a change of 0.01 absorbance units. Less sensitive than the  $12,700 \text{ cm}^{-1}$  band, the  $6,000 \text{ cm}^{-1}$  band can be used to finely discriminate among concentration variations for  $\text{Ti}^{3+}$ . A dashed trendline has been included on the calibration curve to identify the best fit if a zero y-intercept is imposed on the system. It is not apparent that such a requirement is appropriate given that the

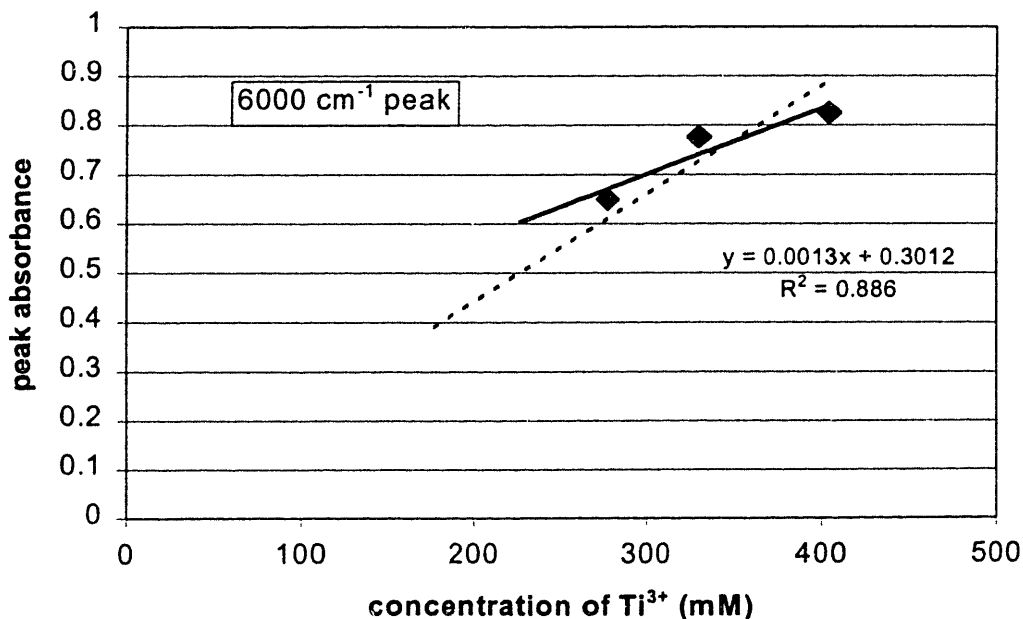


**Figure 36: Calibration curve for the absorption peak at  $6000 \text{ cm}^{-1}$ . Dotted line is the trendline calculated for the data using the origin as an intercept. Temperature is  $688^\circ\text{C}$ .**

6,000  $\text{cm}^{-1}$  band is a band associated with the four-coordinate species, the concentration of which is temperature dependent. Even with the y-intercept requirement, this calibration curve has a less steep slope ( $2.2 \times 10^{-3}$  compared to  $4.2 \times 10^{-3}$ ) and as such is less sensitive to variations in  $\text{Ti}^{3+}$  concentration.

In trying to judge the appropriateness of absorption spectroscopy as a concentration sensor for the chlorotitanates, it is important to assess whether changes in the concentration of  $\text{Ti}^{3+}$  and  $\text{Ti}^{2+}$  can be detected in real time. With two strong peaks in the  $\text{Ti}^{3+}$  spectrum, there is an opportunity for such discriminatory power to be exercised by the system. There are three ways that such system could work. The first option is the most straightforward. One or both of the peaks could be preferentially affected (positively or negatively) by the addition of  $\text{Ti}^{2+}$  to the system. Therefore, it would be possible to track the ratio of the two peak heights and a significant change in that ratio would indicate a change in the  $\text{Ti}^{2+}$  to  $\text{Ti}^{3+}$  ratio. Analyzing peak height ratios on the spectra reported above for the addition of  $\text{Ti}^{2+}$  to a  $\text{Ti}^{3+}$ -rich system produces Figure 37. The ratio of  $\text{Ti}^{2+}$  to  $\text{Ti}^{3+}$  is plotted on the x-axis while the ratio of the 12,700  $\text{cm}^{-1}$  to 6,000  $\text{cm}^{-1}$  peak heights is plotted on the y-axis. The data do not indicate any discernible trend over the range of compositions investigated. The ratio fluctuates around an average value just larger than two, hence this option is not practical.

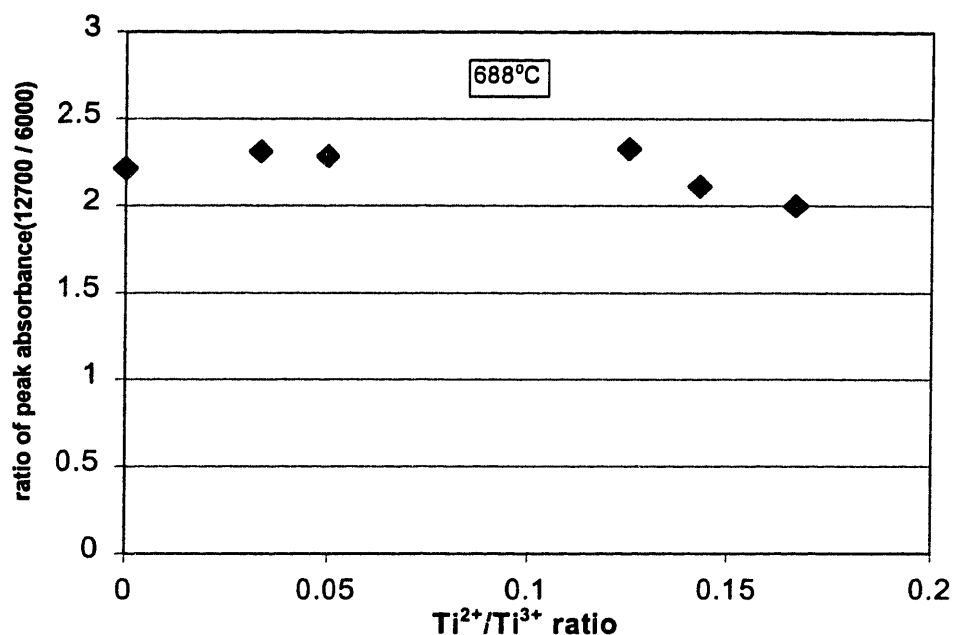


**Figure 37: Peak ratio of the 12,700cm<sup>-1</sup> band to the 6,000 cm<sup>-1</sup> band for the various ratios of Ti<sup>3+</sup> and Ti<sup>2+</sup>. Temperature is 688°C.**

The last two options rely on the fact that Beer's law follows the principle of additivity—in a solution of more than one light-absorbing species each contributes additively to the total absorbance at any particular wavelength. As Sørliie and Øye showed in their previous work, the Ti<sup>2+</sup> spectrum has its two characteristic peaks located at energies very close to the absorption bands in the Ti<sup>3+</sup> spectrum (13,500 cm<sup>-1</sup> and 6,400 cm<sup>-1</sup> for Ti<sup>3+</sup> compared to 13,550 cm<sup>-1</sup> and 6,950 cm<sup>-1</sup> for Ti<sup>2+</sup>). Consequently, the desired discrimination is inherently unlikely for this system. The certain path toward identifying valence shifts is to exploit the law of additivity and after establishing a starting composition track changes in peak height as relative changes in composition. This is termed option three as it is the failsafe option, which is less elegant but still effective.

The intermediate option still relies on the law of additivity, but exploits the temperature sensitivity of the absorption bands. The  $\text{Ti}^{3+}$  spectrum has one temperature sensitive band, while both of the  $\text{Ti}^{2+}$  bands are insensitive to changes in temperature. Since the low energy absorption band for  $\text{Ti}^{3+}$  increases with increasing temperature, it would be expected that the most profound effect of  $\text{Ti}^{2+}$  addition on the peak ratios should be observed for low temperatures. Figure 38 shows the peak height ratios for  $580^\circ\text{C}$  across the range of compositions. The trend is clear and encouraging—the ratio shifts significantly over a short range of composition. The sensitivity of the ratio test is not as strong as the peak height analysis provided above. However, it provides access to the dynamic shifts in composition that are important

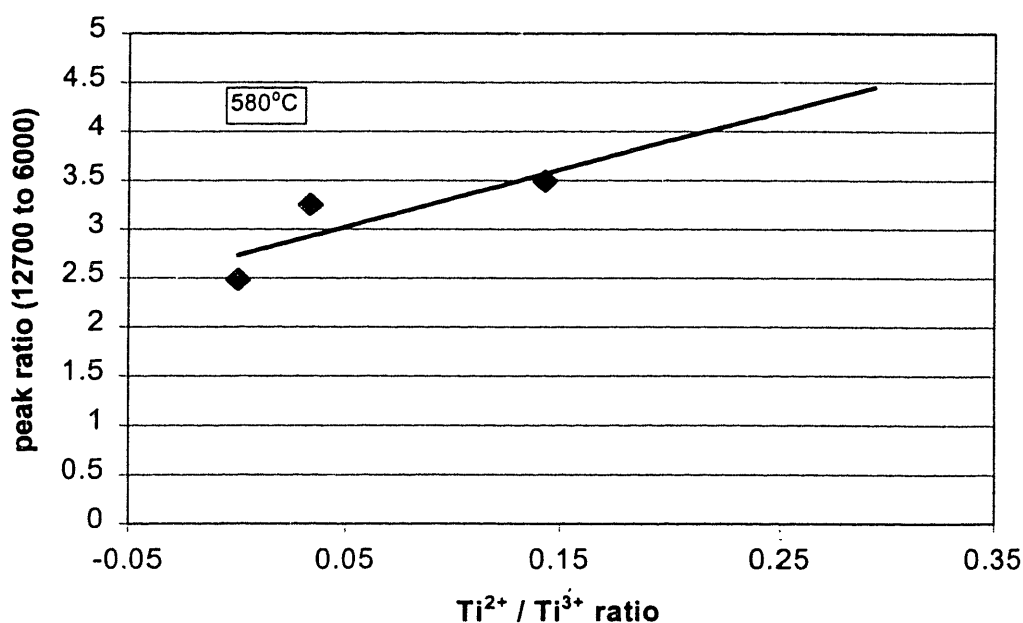


**Figure 38: Peak height ratio for  $12,700\text{ cm}^{-1}$  and  $6,000\text{ cm}^{-1}$  at various ratios of  $\text{Ti}^{3+}$  and  $\text{Ti}^{2+}$ . Temperature is  $580^\circ\text{C}$ .**

industrially and for possible sensor applications (which will be discussed in Chapter 4).

### **3.7 SUMMARY OF SCIENTIFIC FINDINGS**

The spectroscopic investigation and the corresponding analysis produced the following results:

1. Recorded the solid state Raman spectra for  $Ti^{4+}$  and  $Ti^{3+}$ -containing species.
2. Reported the absorption spectra for  $TiCl_3$  while varying concentration and temperature.
3. Confirmed that  $Ti^{3+}$  behaves in a similar manner spectroscopically, in both the CsCl-NaCl-KCl and LiCl-KCl eutectic systems.
4. Determined the concentration calibration curve for  $Ti^{3+}$  at 688°C. Sensitivity to concentration fluctuations was determined to be  $\pm 1$  mM for the  $12,700\text{cm}^{-1}$  peak and  $\pm 5$  mM for the  $6,000\text{cm}^{-1}$  peak.
5. With the goal of developing non-invasive, on-line, real time sensing technologies, identified techniques for using absorption spectra as a concentration sensor for fused salts containing  $Ti^{3+}$  and  $Ti^{2+}$ .

## **4.0 Sensor Recommendations**

### **4.1 POSSIBLE TECHNOLOGIES**

#### *Electrochemical*

The electrochemical techniques employed here have been very helpful in characterizing the kinetics of the electrode reactions. The sensitivity of these techniques to concentration is much improved over dc methods in the high temperature case, as evidenced by the detection of the dissolved titanium gas peak. However, the correlation between peak ac current and concentration of electroactive species was unsatisfactory. It would seem reasonable to assume that because this technology is unmanageable in the laboratory scale, the prospects for its application in industrial systems are poor.

Based on the analysis of the relative values of the relevant rate constants, tight control of the overpotential is one method for avoiding deleterious side reactions such as the redox looping and deposition of undesirable metal impurities. Hence, industrial implementation of a high temperature  $\text{Ag}/\text{Ag}^+$  reference electrode such as the ones employed in the present study would be beneficial. Not only would this serve as an on-line control of overpotential, but it would also provide valuable diagnostic information about the process, potential variation over time and the ratio of cathodic to anodic potential at constant current.

### *Raman spectroscopy*

At the beginning of the present study, the application of vibrational spectroscopy to characterize the bulk structure of the molten chlorotitanates in real time appeared to be an attractive possibility. Previous work on transition metal chlorides in this laboratory as well as by others provided much of the reason for optimism. However, the molten chlorotitanates have certain spectral characteristics that prevent effective use of Raman methods. Typical concentrations for Raman detection produced melts that were deeply colored such that any signal generated by the chloro-complexes was re-absorbed by the melt. In addition, lowering the concentration decreased the signal intensity. In sum, these complications point out that the technology is ill suited to application in the present system.

### *Absorption spectroscopy*

After recognizing the limitations to investigation with vibrational spectroscopic techniques, the study turned to absorption spectroscopy. In this technique, the deeply colored nature of the melts is an asset and the results indicate how the response due to electronic transitions gives an accurate determination of the amount of  $Ti^{3+}$  present as well as identifying the addition of  $Ti^{2+}$ . The results indicate that the fiber optic assembly can be employed without hindering the detection capabilities of the technique. The technique is not only quantitative, but the detection limits are low enough that variation of less than 10 mM is easily detected. If the industrial system allows flexibility in

operating temperature, then lowering the temperature should allow implementation of a fiber optic on-line control to detect changes in the ratio of  $Ti^{2+}$  and  $Ti^{3+}$ .

#### **4.2 SPECULATION ON IMPROVEMENTS TO THE TECHNOLOGY**

If the relative values of the rate constants can be adjusted so as to make  $Ti^{3+}/Ti^{2+}$  the slow step, the current inefficiencies due to redox looping become less significant. A self correcting mechanism develops so that the cathodic process consumes all  $Ti^{2+}$  that develops as soon as it is in the vicinity of the central electrode.

With  $k^0$  having an Arrhenius relationship to temperature, changing operating temperatures will affect  $k^0$ . However, the effect is nearly similar for each reaction since both  $k^0$  values scale with temperature. It is also possible to change  $k^0$  by changing the electrode employed hoping that the relative values of  $k^0$  will grow closer if not switch. A change in the electrode material or the nature of its surface will also cause a change in  $\alpha$ , which effects the forward and reverse rate constants ( $k_f$  &  $k_b$ ) and hence the actual rates of forward and reverse reaction ( $v_f$  &  $v_b$ ). In this situation, it is desired to select an electrode that decreases  $\alpha$  for  $Ti^{3+}/Ti^{2+}$  and increases  $\alpha$  for  $Ti^{2+}/Ti^0$ .



## **5.0 Conclusions**

### **5.1 SYNTHESIS OF CONCLUSIONS IN CHAPTER 2, 3 AND 4**

As a result of this work, the kinetics of the electrorefining reactions are now known. In particular, the transfer coefficient and standard rate constant for the  $\text{Ti}^{3+}/\text{Ti}^{2+}$  and  $\text{Ti}^{2+}/\text{Ti}^0$  couples have been determined. Additionally, the  $\text{Ti}^{2+}/\text{Ti}^0$  step has been identified as the slow step. Melt speciation has been characterized by spectroscopic methods which have also shown promise for determination of the AEV of titanium for on-line control.

The new kinetic information not only helped to characterize the system, but also provides an explanation for some of the empirically observed “rules.” The ratio of  $k^0$  for  $\text{Ti}^{3+}/\text{Ti}^{2+}$  to  $k^0$  for  $\text{Ti}^{2+}/\text{Ti}^0$  may explain the empirically determined ideal bath ratio of 2.1 AEV. The different  $\alpha$  values provide an understanding of the interplay between the electrode materials and the ions involved in a faradaic process. Through proper choice of electrode materials (based on the relationship between their work function and the Fermi levels in the ionic couple) the kinetic performance of a faradaic system can be engineered to produce desired results.

The present investigation shows the power of ac methods to reveal reaction kinetics under conditions that render dc methods impotent. This is particularly true in high temperature molten salt systems where previously it was almost impossible to gain access to reliable kinetic information about technologically important faradaic processes. There is nothing peculiar about

the way the chlorotitanate study was conducted that would indicate that the approach cannot be generalized and employed in the study of other aliovalent systems at high temperature.

## **5.2 RECOMMENDATIONS FOR FUTURE WORK**

The success of the present study has opened many opportunities for future investigation not only in the chlorotitanates, but also in other systems.

In the chlorotitanates studies include:

- determination of kinetic constants on an inert WE other than glassy carbon (eg. tungsten, platinum, or gold) and possibly on an active titanium WE;
- impedance work to determine an overall equivalent circuit;
- spectroelectrochemical analysis to combine the techniques in the same cell.

The present study indicates that a better understanding the nature of the disproportionation reaction between  $Ti^{2+}$  and  $Ti^{3+}$  would be valuable. This includes knowledge of:

- forward and reverse reaction rates;
- temperature dependence of the reaction; and
- the influence of potential;

with the goal of trying to determine if the reaction can be suppressed or avoided.

There are distinct possibilities for using the promising on-line control techniques as both industrial controls and diagnostic tools. Such industrial based work would include:

- developing a fiber optic probe for studying the *in situ* absorption behavior of industrial melts;
- converting the lab scale  $Ag/Ag^+$  reference to industrial scale;
- implementing the reference in production electrorefining cells and measuring the anodic and cathodic potentials for the first time while also tracking them over the period of a run and production campaign;
- after developing the absorption probe and calibrating in the industrial melt, tracking the AEV during a run and campaign leading to hypotheses about the periods of poor efficiency.

As for extending the work to other aliovalent and commercially important molten salt systems:

- studies of aluminum production especially the  $\text{Al}^{3+}/\text{Al}^0_{(l)}$  couple;
- determination of the kinetics of the reduction of transition metal chlorides including those of zirconium, hafnium, chromium, tantalum, and vanadium;
- studies of the kinetics of production of alkali and alkaline-earth metals, e.g., lithium, sodium, potassium, or magnesium.

## Bibliography

- Adams, D.M. and D.C. Newton, *J. Chem. Soc.(A): Inorg. Phys. Theor.*, (1968) 2262.
- Bard, A.J. and L.R. Faulkner, *Electrochemical Methods*, John Wiley & Sons, New York, 1980.
- Bulmer, J.T. and H.F. Shurvell, *The Journal of Physical Chemistry*, 77 (1973) 256 and 2085.
- Baboian, R., D.L. Hill and R.A. Bailey, *Canadian Journal of Chemistry*, 43 (1965) 197.
- Bernard, C., M. Pons, E. Blanquet, and R. Madar, *MRS Bulletin*, 24:4 (1999) 27.
- Calvo, E.J., "Fundamentals: The Basics of Electrode Reactions" in *Comprehensive Chemical Kinetics*, vol. 26: *Electrode Kinetics: Principles and Methodology*, New York: Elsevier, 1986.
- Chassaing, E., F. Basile and G. Lorthioir, *Journal of the Less-Common Metals*, 68 (1979) 153.
- \_\_\_\_\_, *Ann. Chim. Fr.*, (1979) 295.
- \_\_\_\_\_, *Titanium '80 Science and Technology: Proceedings of the Fourth International Conference on Titanium*, (1980) 1963.
- Chassaing, E., G. Lucazeau and G. Lorthioir, *Z. Anorg. Allg. Chem.*, 468 (1980) 235.
- Chassaing, E., F. Basile and G. Lorthioir, *Journal of Applied Electrochemistry*, 11 (1981) 187.
- \_\_\_\_\_, *Journal of Applied Electrochemistry*, 11 (1981) 193.
- Clark, R.J.H., L. Maresca and R.J. Puddephatt, *Inorganic Chemistry*, 7 (1968) 1603.
- Clayton, F.R., G. Mamantov and D.L. Manning, *Journal of the Electrochemical Society: Electrochemical Science and Technology*, 120 (1973) 1193.
- Creighton, J.A. and J.H.S. Green, *J. Chem. Soc.(A): Inorg. Phys. Theor.*, (1968) 808.
- Crouch, P.C., G.W.A. Fowles and R.A. Walton, *J. Chem. Soc.(A): Inorg. Phys. Theor.*, (1969) 972.
- Dai, S., J.P. Young, G.M. Begun, J.E. Coffield and G. Mamantov, *Mikrochimica Acta*, 108 (1992) 261.

- Dai, S., G.M. Begun, J.P. Young and G. Mamantov, *Journal of Raman Spectroscopy*, 26 (1995) 929.
- Driscoll, K.J. and D.J. Fray, *EPD Congress 1992*, The Minerals, Metals & Materials Society, (1991) 1345.
- Ferraro, J.R. and K. Nakamoto, *Introductory Raman Spectroscopy*, Academic Press, Boston, MA, 1994.
- Ferry, D.M., G.S. Picard and B.L. Tremillon, *Proceedings of the Joint International Symposium on Molten Salts*, The Electrochemical Society, (1987) 517.
- Flengas, S.N. and T.R. Ingraham, *Canadian Journal of Chemistry*, 35 (1957) 1139.
- \_\_\_\_\_. , *Canadian Journal of Chemistry*, 35 (1957) 1254.
- \_\_\_\_\_. , *Canadian Journal of Chemistry*, 36 (1958) 780.
- \_\_\_\_\_. , *Canadian Journal of Chemistry*, 36 (1958) 1103.
- \_\_\_\_\_. , *Journal of the Electrochemical Society*, 106 (1959) 714.
- \_\_\_\_\_. , *Canadian Journal of Chemistry*, 38 (1960) 813.
- Flengas, S.N., *Annals of New York Academy of Sciences*, (1960) 853.
- Fraser, G.V., J.M. Chalmers, V. Charlton and M.E.A. Cudby, *Solid State Communications*, 21 (1977) 933.
- Girginov, A., T.Z. Tzvetkoff, and M. Bojinov, *Journal of Applied Electrochemistry*, 25 (1995) 993.
- Grjotheim, K., C. Krohn, M. Malinovsky, K. Matiasovsky and J. Thonstad, *Aluminum Electrolysis: Fundamentals of the Hall-Heroult Process*, Aluminum-Verlag, Dusseldorf, 1982.
- Gruen, D.M. and R.L. McBeth, *Pure Appl. Chem.*, 6 (1963) 23.
- Haarberg, G.M., W. Rolland, A. Sterten, and J. Thonstad, *Journal of Applied Electrochemistry*, 23 (1993), 217.
- Kipouros, G.J., J.H. Flint and D.R. Sadoway, *Inorganic Chemistry*, 24 (1985) 3881.
- Korol'kov, D.V. and G.N. Kudryashova, *Russian Journal of Inorganic Chemistry*, 13 (1968) 850.
- Lister, R.L. and S.N. Flengas, *Canadian Journal of Chemistry*, 41 (1963) 1548.
- Menzies, I.A., D.L. Hill, G.J. Hills, L. Young and J.O'M. Bockris, *Journal of Electroanalytical Chemistry*, 1 (1959/60) 161.

- MetalPrices.com LLC, (2000), *Titanium, Aluminum, & Iron*, [Online], Available: <http://metalprices.com> [2000, May 1].
- Morozov, I.S. and D.Ya. Toptygin, *Russian Journal of Inorganic Chemistry*, 5 (1960) 42.
- Nardin, M. and G. Lorthioir, *Journal of the Less-Common Metals*, 56 (1977) 269.
- Oki, T., M. Okido and C. Guang-Sen, *Proceedings of the Joint International Symposium on Molten Salts*, The Electrochemical Society, (1987) 507.
- Petrushina, I., Danish Technical University, Denmark , Private Communication, 11 February 2000.
- Popov, B.N., M.C. Kimble, R.E. White and H. Wendt, *Journal of Applied Electrochemistry*, 21 (1991) 351.
- Reid, W.E. Jr., *Journal of the Electrochemical Society*, 108 (1961) 393.
- Schwab, S.D. and R.L. McCreery, *Anal. Chem.*, 56 (1984) 2199.
- Sequeira, C.A.C., *Journal of Electroanalytical Chemistry*, 239 (1988) 203.
- Smirnov, M.V., V.S. Maksimov and A.P. Khaimenov, *Russian Journal of Inorganic Chemistry*, 11 (1966) 945.
- Sørli, M. and H.A. Øye, *Inorganic Chemistry*, 17 (1978) 2473.
- Sørli, M. and H.A. Øye, *Inorganic Chemistry*, 20 (1981) 1384.
- Tumidajski, P.J. and S.N. Flengas, *Journal of the Electrochemical Society*, 138 (1991) 1659.
- van Bronswyk, W., R.J.H. Clark and L. Maresca, *Inorganic Chemistry*, 8 (1969) 1395.
- Wendling, E. and R. Rohmer, *Bulletin de La Societe Chimique de France*, (1967) 8.
- Wurm, J.G., L. Gravel and R.J.A. Potvin, *Journal of the Electrochemical Society*, 104 (1957) 301.

## **Biographical Note**

The author was born in Jacksonville, N.C. at the Camp LeJeune Marine Base. Luis was raised in Pensacola, FL with summers being spent in Newcomerstown, OH on his grandparents farm. In the summer of 1991, Luis was selected as one of approximately 60 high school juniors to attend MIT's Minority Introduction To Engineering and Science (MITES) Program. A state champion in speech and debate, Luis earned the International Baccalaureate degree upon completion of the program at Pensacola High School in June of 1992. Matriculation for the fall of 1992 at MIT was a natural.

As an undergraduate, Luis majored in Materials Science and Engineering and earned a minor in political science. As a part of the 3B internship program, Luis spent his summers working north of Pittsburgh, PA at The ALTA Group, A Johnson Matthey Company in Fombell, PA. Luis was a four year member of the Heavyweight Crew team at MIT and as such spent far too much time at the boathouse and on the water (estimated at more than 24 hours a week). Yet, he still managed to garner admission to MIT's graduate program in Materials Science and Engineering. This internship relationship turned out to be a great connection as the company was cultivated to sponsor research at MIT after consultation with Professor Donald Sadoway.

As a graduate student, Luis continued to progress academically while maintaining an active involvement in campus life. Serving as the graduate student member on MIT's Presidential Task Force on Student Life and Learning, Luis gained a unique insight into education at MIT. Leading a Student Advisory Committee which pushed the Task Force along in its work, Luis was able to help the committee shape its concept of MIT's ideal educational structure – the Educational Triad – and develop a consensus among the Task Force members that this was MIT's path to the future. After two years of service on the Task Force, as well as founding and growing the Student Ambassador Program in parallel, Luis continued his participation in student involvement, putting that knowledge learned in his graduate management minor to use. Serving as student liaison to the Boston Chapter of ASM, Luis helped raise the level of student involvement in the society and developed a new series of Student Desert talks. Continuing his interest in Institute governance, Luis joined other interested students and MIT's Chancellor, Larry Bacow, to establish a Strategic Advisory Committee for students to stay involved in educational strategy discussions.



In the final year of his time at MIT, Luis raised his level of engagement. Serving as president of the Graduate Student Council, Luis formalized his involvement in policy making. Additionally, his level of professional engagement increased as well. Serving as a part time consultant to develop ideas for a new titanium refining process at ALTA, Luis saw the industrial side of process conception and design. As the results of the thesis work came into focus, presentations at professional conferences became obligatory (1999 and 2000 TMS Conference and Fall 1999 Meeting of the Electrochemical Society).

Splitting time on campus, at the research sponsor and at Oak Ridge National Laboratory, Luis certainly saw different faces of the research science industry. Industry, academe or science policy....which will be next?

**Luis A. Ortiz**

# THESIS PROCESSING SLIP

FIXED FIELD: ill \_\_\_\_\_ name \_\_\_\_\_

index \_\_\_\_\_ biblio \_\_\_\_\_

► COPIES: Archives Aero Dewey Eng Hum  
Lindgren Music Rotch Science

TITLE VARIES: ►  \_\_\_\_\_

NAME VARIES: ►  Anthony

IMPRINT: (COPYRIGHT) \_\_\_\_\_

► COLLATION: \_\_\_\_\_

► ADD: DEGREE: \_\_\_\_\_ ► DEPT.: \_\_\_\_\_

SUPERVISORS: \_\_\_\_\_

NOTES:

cat'r

date

page

► DEPT: Math & E. ► JHEW

► YEAR: 2000 ► DEGREE: Ph.D.

► NAME: CPH 11 A.